FRONTIERS OF PHYSICS

TOPICAL REVIEW
Volume 21 / Issue 12 / 125301 / 2026

Electrical and magnetic transitions in $FeSb_2$: A critical review of competing microscopic pictures

Huayao Li, Xiaoqian Zhang†, Lin Miao‡

Key Laboratory of Quantum Materials and Devices of Ministry of Education, School of Physics, Southeast University, Nanjing 211189, China
Corresponding authors. E-mail: †zhangxq@seu.edu.cn, ‡lmiao@seu.edu.cn
Received January 5, 2026; accepted March 27, 2026

ABSTRACT

Iron antimonide ($FeSb_2$) is a prototypical correlated narrow-gap system that exhibits a metal–insulator-like crossover and a concomitant diamagnetic-to-paramagnetic transition. However, the microscopic physical origin of these anomalous electrical and magnetic behaviors has been the subject of a long-standing debate. Two competing physical pictures have been proposed: the Kondo insulator (KI) framework, which attributes the gap formation to Kondo hybridization, and the spin-state excitation (SSE) mechanism, which emphasizes a thermally activated transition from a low-spin state to a high-spin state. In this review, we provide a critical overview of key experimental results from electrical transport, magnetic properties, and a broad range of spectroscopic probes, assessing how each supports or challenges these competing physical pictures. Particular attention is paid to recent advances in element- and orbital-sensitive spectroscopies, such as X-ray absorption spectroscopy (XAS), which together offer direct insights into the evolution of the Fe spin state and electronic structure. Additional anomalous properties, such as the colossal thermoelectric effect and spin-structure instabilities, are also discussed in the end. These emerging features not only underscore the complexity of this correlated narrow-gap system but also suggest rich, unresolved physics beyond existing models, inviting further investigation into its fundamental behavior and potential applications.

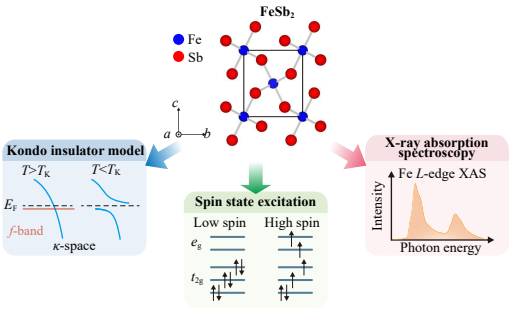

Keywords narrow-gap semiconductor, metal–insulator-transition, spin-state excitation, Kondo effect, X-ray absorption spectroscopy

Contents

Higher Education Press

https://doi.org/10.15302/frontphys.2026.125301

1 Introduction

Narrow-gap semiconductors have emerged as a prominent research frontier in condensed matter physics and materials science due to their unique electronic structures and tunable physical properties [1–3]. These materials typically exhibit bandgaps on the order of several hundred millielectronvolts (meV), corresponding to excitation energies within the infrared (IR) regime, making them widely applicable in fields such as infrared photodetection, remote sensing, and low-power IR devices [4–10]. For instance, indium antimonide (InSb, bandgap ~ 0.17 eV) exhibits high sensitivity to infrared radiation in the 1–5 μm wavelength range, making it a key material for cryogenic short-wave infrared (SWIR) detectors [11, 12]. On the other hand, the large carrier effective masses in narrow-gap semiconductors can yield Seebeck coefficients that greatly exceed those of metals and wide-gap semiconductors. When combined with tunable carrier densities, this facilitates the achievement of a high thermoelectric figure of merit, $ZT = S^2\sigma T/\kappa$, where S, σ, T, and κ represent the Seebeck coefficient, electrical conductivity, absolute temperature, and total thermal conductivity, respectively [1]. A paradigmatic case is Bi_2Te_3 (bulk bandgap ~ 0.15 eV) [13], whose large Seebeck coefficient and intrinsically low lattice thermal conductivity make it one of the most outstanding thermoelectric materials near room temperature and have enabled its deployment in commercial solid-state cooling devices [14–17].

Although narrow-gap semiconductors have achieved significant applications in infrared technology and thermoelectric, current research actively searches for new narrow-gap compounds that exhibit unconventional electronic or thermoelectric behavior, with the goal of extending operating temperature ranges, improving efficiencies, introducing new functionalities, and reducing reliance on rare-earth elements [18]. While most established narrow-gap materials can be optimized through band engineering and doping, their physical properties largely define by the bandgap within the single-particle picture without any electronic correlations. To move beyond this conventional framework of semiconductors, research attention is shifting toward non-trivial topology, reduced dimensionality, and strong electronic correlations. These systems may leverage many-body effects to achieve superior or novel functionalities, catering to more extreme application demands. Among these emerging candidate materials, iron diantimony ($FeSb_2$) has attracted considerable interest due to the series of anomalous physical properties observed at low temperatures [1].

Initially, $FeSb_2$ was regarded as a conventional narrow-gap semiconductor. Subsequent studies revealed that it exhibits a record-breaking Seebeck coefficient, reaching approximately 45 mV/K at around 10 K, which far exceeds conventional theoretical predictions [19]. Such an exceptional thermoelectric response suggests immense potential for thermoelectric applications. If the lattice thermal conductivity can be effectively suppressed, the thermoelectric figure of merit could be significantly enhanced, enabling the material to play a pivotal role in solid-state cryogenic cooling and thermoelectric power generation in the extreme low-temperature regime.

Since the discovery of its exceptionally large low-temperature thermoelectric response, $FeSb_2$ has drawn sustained attention from both the condensed-matter and thermoelectric communities. Early studies focused mainly on the microscopic origin of this remarkable macroscopic behavior, leading to extensive discussion of mechanisms such as carrier excitation, correlation-driven renormalization, and phonon drag. At the same time, considerable effort has been directed toward improving its thermoelectric performance through elemental substitution, defect control, and nanostructure engineering aimed at reducing lattice thermal conductivity and enhancing the thermoelectric figure of merit [20–28]. More recently, the scope of $FeSb_2$ research has expanded significantly. Between 2020 and 2025, conceptual and experimental approaches from topological quantum materials, strongly correlated electron physics, and X-ray spectroscopy have increasingly been applied to this system. Meanwhile, the emergence of ideas such as altermagnetism has renewed interest in spin-dependent phenomena in transition-metal compounds and has opened additional perspectives for understanding the electronic structure and magnetism of $FeSb_2$. As a result, current research extends well beyond phonon drag and thermal transport to encompass issues such as surface-bulk separation and correspondence, lattice dynamics, and their consequences for electronic structure and charge transport [29–36].

Beyond its thermoelectric behavior and these newly emerging directions, $FeSb_2$ also exhibits a range of unusual fundamental properties reminiscent of strongly correlated electron systems. Although $FeSb_2$ exhibits anisotropic magnetic susceptibility at low temperatures, it shows diamagnetic ($H||(001)$) or nonmagnetic (H is along other direction) at the low temperature [37]. With the temperature ramping up, the magnetic response get profoundly enhanced to paramagnetic at temperature around 100 K. Correspondingly, its electrical resistivity exhibits a temperature-controlled metal–insulator-like transition. These behaviors are highly analogous to those of classic correlated semiconductors with Kondo interaction, such as SmB_6 and FeSi, suggesting the existence of

a novel electronic state in $FeSb_2$ dominated by electron correlations [38–40]. Therefore, elucidating the microscopic origin of $FeSb_2$'s anomalous properties is crucial for both advancing our fundamental understanding of correlation-driven phenomena and guiding the rational design of materials with tailored functionalities.

This review provides a systematic overview of the intriguing physical phenomena in $FeSb_2$, with the aim of developing a comprehensive understanding of this material and offering insights into other correlated semiconductors with similar properties. The article is organized as follows. Section 2 introduces the puzzling and exotic properties of $FeSb_2$ and summarizes the proposed physical explanations. Section 3 focuses on the physics of phase transitions, examining interpretations based on the Kondo insulator (KI) model and comparing $FeSb_2$ with representative Kondo materials such as SmB_6. Section 4 reviews alternative theoretical models, mainly the spin-state excitation (SSE) hypothesis, and provides a systematic analysis of ongoing controversies. Section 5 concentrates on microscopic evidence from recent spectroscopic probes, including X-ray absorption and photoemission spectroscopy, and discusses the constraints on theoretical models. Finally, Section 6 outlines future research directions for $FeSb_2$, highlighting potential applications in thermoelectricity, spintronics, and novel magnetic phenomena like altermagnetism. By integrating these interconnected aspects, this review aims to elucidate the rich and nontrivial physics hidden within this seemingly simple material and to offer perspectives on future research directions.

2 Unusual physical properties of $FeSb_2$

$FeSb_2$ exhibits unusually strong sensitivity of its transport properties to subtle variations in microscopic disorder and sample conditions, including stoichiometric deviations, residual impurities or defects, strain, and growth conditions. As a result, transport and magnetic measurements reported in the literature can differ qualitatively even among nominally similar samples. Unless otherwise stated, the following discussion of macroscopic transport behavior and microscopic modeling takes high-quality, near-intrinsic single crystals as the reference case.

2.1 Anomalous electrical transport

$FeSb_2$ crystallizes in the orthorhombic marcasite structure with the space group *Pnnm* [Fig. 1(a)] [41]. While early studies on polycrystalline $FeSb_2$ suggested it as narrow-gap semiconductor, the successful growth of high-quality single crystals in the early 2000s revealed a far more complex physical behavior. A notable feature of $FeSb_2$ is its profound anisotropy in electrical transport. Petrovic *et al.* [42] demonstrated that while the resistivity along the a and c axis exhibits typical semiconducting behavior ($d\rho/dT < 0$) over the entire temperature range, the R–T along b-axis behaves in a qualitatively different manner. Along this axis, the resistivity is metallic ($d\rho/dT > 0$) at high temperatures, passes through a minimum around $T_{min} \sim 40$ K, and subsequently evolves into insulating-like behavior upon further cooling. However, not all reports reproduce a stark divergence among the three crystallographic axes. Some measurements [19, 43] have instead observed nearly isotropic semiconducting behavior along all axes down to low temperatures, arguing that the large anisotropy and the metallic segment along b-axis may depend sensitively on subtle structural distortions or sample-specific differences (e.g., strain, defects) [Fig. 1(c)]. Later on, Raman spectroscopy, identified the phonon anomaly along the b-axis at $T \sim 100$ K, indicating a possible lattice distortion along the b-axis [44]. Thus, one must treat the metal to insulator transition along the b-axis with caution, acknowledging possible the sample-dependence due to possible off-stoichiometry effect.

Detailed analysis of the temperature-dependent resistivity revealed the presence of multiple energy scales. Through the fitting analysis of Arrhenius equation, several research groups independently identified two distinct thermal activation energy gaps. A larger gap (Δ_1) of ~ 30–40 meV is observed at higher temperatures ($T > 30$ K) and is typically associated with the intrinsic semiconductor band gap. Below this temperature, however, a much smaller gap (Δ_2) of ~ 6–10 meV dominant the transport behaviors [42, 45, 46]. The origin of this smaller gap remains an open question. Although it was initially suspected to be an impurity band, its reproducible observation in high-purity crystals suggests that it is possibly an intrinsic feature and may be associated with Kondo-like hybridization, a topic explored later in this review.

The most enigmatic feature is a distinct resistivity saturation plateau observed below 10 K, a feature inconsistent with simple semiconducting models. For years, the origin of this plateau was debated, as conventional four-probe measurements could not separate bulk from potential surface contributions. A breakthrough came from Corbino-disk geometry experiments [47], which isolate bulk conduction from surface paths, demonstrated that the bulk resistivity of $FeSb_2$ does not saturate but continues to increase exponentially upon cooling. This compelling result proves that the bulk of $FeSb_2$ is truly insulating and that the observed resistivity plateau is definitively caused by highly conductive metallic surface channels. This finding has fundamentally shifted the focus of the field. The central question is no longer whether non-bulk conduction channels exist or not, but rather what the exactly nature of these conductive surface states is and whether they possess non-trivial topological character [38, 48].

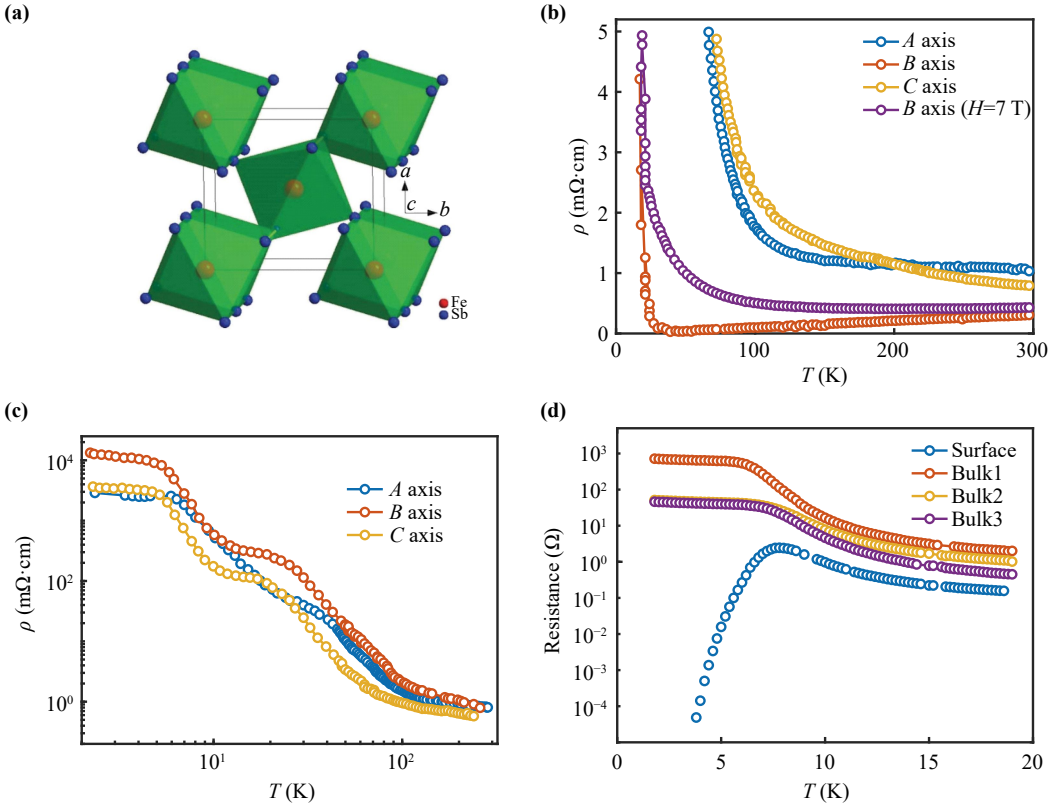

Fig. 1 **(a)** Marcasite-type crystal structure of $FeSb_2$, where Fe atoms embedded in a framework of Sb octahedra (Ref. [41]). **(b)** Temperature dependence of the resistivity $\rho(T)$ measured along the *a*-, *b*-, and *c*-axis. The resistivities along the *a*- and *c*-axes display typical semiconducting behavior, whereas the resistivity along the *b*-axis exhibits a distinct metal–insulator crossover with a minimum at $T \sim 40$ K. Upon applying a magnetic field of $H = 7$ T, the semiconducting-like behavior is restored. Reproduced from Ref. [42]. **(c)** The $\rho(T)$ along the three axes for another $FeSb_2$ single crystal, showing semiconducting behavior on all axes and lacking the metallic anomaly along the *b* axis, in contrast to panel (b). Reproduced from Ref. [19]. **(d)** Corbino-disk measurement of bulk and surface transport in $FeSb_2$. The surface resistivity shows a decrease at low temperatures, indicating the emergence of an additional conducting channel localized near the sample surface. Reproduced from Ref. [47].

2.2 Temperature-dependent magnetic susceptibility

Complementing the complex electric transport phenomena, the magnetic properties of $FeSb_2$ provided the evidence for the possible role of strong electron correlations. Systematic measurements of the magnetic susceptibility [$\chi(T)$] on high-quality single crystals revealed a highly unconventional temperature dependence [Fig. 2(a)] [42, 49]. At low temperatures, the system is diamagnetic with a nearly flat, negative susceptibility. As the temperature increases, $\chi(T)$ crosses over to a paramagnetic state, passing through a broad maximum centered around 100 K before following a Curie-Weiss-like behavior at higher temperatures. This characteristic behavior has since been confirmed in numerous studies, including those under high pressure which showed the feature to be robust but tunable [Fig. 2(b)] [50].

The paramagnetic anomaly observed in $FeSb_2$ is unexpected given its low-spin Fe configuration ($3d^4$ or $3d^6$), as confirmed by X-ray absorption spectroscopy (XAS) [51]. However, this non-monotonic behavior is strikingly reminiscent of the magnetic signature of the canonical KI candidate, FeSi [52]. In FeSi, both the thermally activated resistivity and the crossover from a low-temperature diamagnetic state to a high-temperature paramagnetic state are well described within a hybridization-gap framework supplemented by dynamical mean-field theory (DMFT), which captures a temperature-driven evolution from a nonmagnetic insulating ground state to a correlated paramagnetic semiconductor [Fig. 2(c)] [53]. The striking similarity between FeSi and $FeSb_2$ therefore indicates a possibly shared microscopic mechanism rooted in strong hybridization and electron–electron correlations that drive gap formation [54]. From this perspective, the magnetic anomaly redefined the classification of $FeSb_2$ from a simple semiconductor to a candidate correlated electron system. This analogy to FeSi has strongly influenced the theoretical understanding ever since, serving as a primary piece of evidence for models based on a Kondo-like hybridization

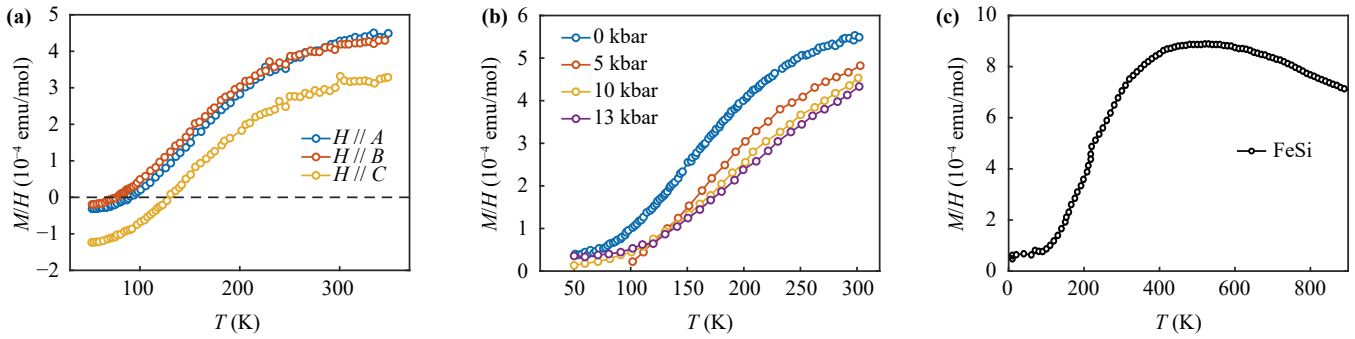

Fig. 2 **(a)** Temperature-dependent magnetic susceptibility $\chi(T)$ of a flux-grown $FeSb_2$ single crystal measured along the *a*, *b*, and *c* axes. All three directions show similar temperature dependences, with a small offset for $H \parallel c$ relative to $H \parallel a$, *b*. Reproduced from Ref. [42]. **(b)** Temperature dependence of the magnetic susceptibility of $FeSb_2$ at various pressures. Compared with ambient pressure, applying pressure suppresses $\chi(T)$ over the measured temperature range while preserving a qualitatively similar temperature dependence. Reproduced from Ref. [50]. **(c)** Magnetic susceptibility $\chi(T)$ of FeSi shown as a reference Kondo insulator, exhibiting a similar temperature dependence for comparison with $FeSb_2$. Reproduced from Ref. [53].

gap–a picture that remains central to the ongoing debate over the material's microscopic origins.

2.3 The colossal Seebeck effect and the thermoelectric dilemma

In addition to its intriguing transport and magnetic behaviors, the observation of a colossal thermoelectric effect has made $FeSb_2$ a material of significant scientific interest. Bentien *et al.* [19] reported in a series of studies that high-quality $FeSb_2$ single crystals exhibit a record-breaking Seebeck coefficient at low temperatures, reaching a peak value of approximately –45 000 μV/K around 10–12 K [Fig. 3(a)]. Combined with the relatively low resistivity in the corresponding temperature range, this resulted in a peak thermoelectric power factor (PF = $S^2\sigma$) as high as 2300 μW/(cm·K^2), a value several tens of times greater than that of state-of-the-art commercial thermoelectric materials like Bi_2Te_3, indicating significant potential for low-temperature refrigeration applications. Based on this, Sun *et al.* [54, 55] showed that $FeSb_2$'s power factor far exceeds that of the isostructural compounds $FeAs_2$ and $RuSb_2$, arguing that the enhancement of *ZT* is intrinsic to the narrow, correlated bands of $FeSb_2$ rather than a universal property of its crystal structure [Fig. 3(a)]. Complementarily, Takahashi *et al.* [56] demonstrated a strong dependence of the Seebeck coefficient on sample size and geometry, with smaller crystals showing enhanced peak values and narrower peak widths around 10 K. This behavior indicates that the thermoelectric response in $FeSb_2$ is markedly influenced by the phonon mean free path and boundary conditions [Fig. 3(b)]. Together, these compelling experimental findings spurred the development of theoretical frameworks in understanding the colossal thermoelectricity in $FeSb_2$. In particular, Tomczak *et al.* [57] involved many-body

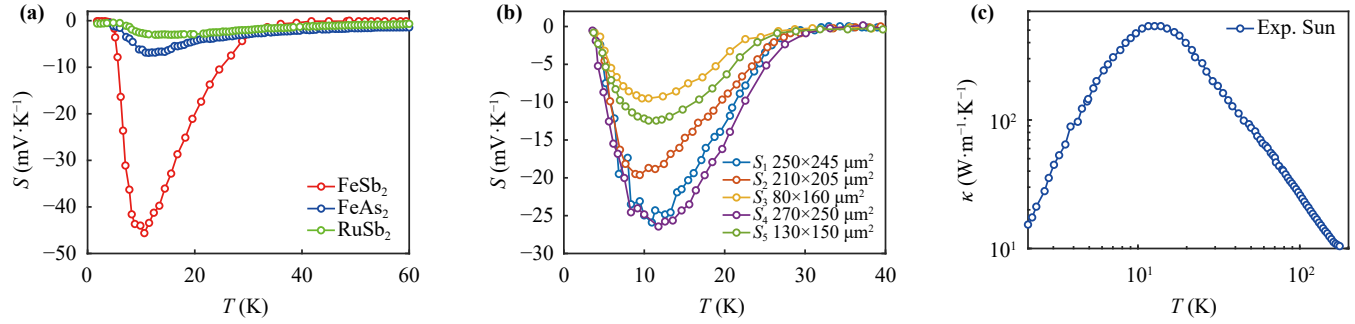

Fig. 3 **(a)** Temperature dependence of the Seebeck coefficient $S(T)$ for $FeSb_2$ [19], $FeAs_2$ [54], and $RuSb_2$ [55]. All three compounds show a low temperature maximum near ~ 10 K, but $FeSb_2$ exhibits a much larger peak value (about one order of magnitude higher than $RuSb_2$ and $FeAs_2$). **(b)** Seebeck coefficient $S(T)$ of $FeSb_2$ measured on samples with different cross-section. The maximum absolute Seebeck coefficient increases with the sample's cross-sectional area, demonstrating that crystal boundary scattering enhances the Seebeck effect. Reproduced from Ref. [56]. **(c)** Thermal conductivity $\kappa(T)$ of $FeSb_2$ single crystals, showing a pronounced low temperature peak in a similar temperature regime to the Seebeck maximum, which contributes to the limitation of the thermoelectric figure of merit *ZT* in $FeSb_2$. Reproduced from Ref. [42].

theory to demonstrate that conventional band pictures cannot reproduce the extreme low-T Seebeck coefficient of $FeSb_2$. They further proposed that vertex corrections (e.g., electron–phonon drag) beyond simple quasiparticle renormalization in the calculation are essential, placing $FeSb_2$ in a distinct regime among correlated semiconductors.

However, despite the enormous efforts of experimental and theoretical work dedicated to understanding its thermoelectric properties, the practical application of $FeSb_2$ remains severely constrained: the thermoelectric figure of merit of $FeSb_2$ is extremely low, calculated to be only about 0.005, far below the practical threshold ($ZT \sim 1$). The primary reason lies in the exceptionally high lattice thermal conductivity (κ) of $FeSb_2$, which also peaks [around 300–550 W/(m·K)] in the same temperature range (~ 15 K) coincidentally [Fig. 3(c)] [41]. This high thermal conductivity facilitates rapid heat flow through the material, severely compromising its ability to establish and maintain a temperature gradient, thus drastically reducing the thermoelectric conversion efficiency. A proper understanding of this thermoelectric dilemma requires an explicit disentanglement between the diffusion and phonon-drag contributions to the Seebeck coefficient. The colossal low-temperature thermopower in $FeSb_2$ is widely attributed to a strong phonon-drag contribution associated with long-lived phonons of long mean free path [58–61]. This provides a microscopic explanation for the apparent trade-off: the same phonon properties that enhance phonon drag also lead to an unusually large lattice thermal conductivity. As a result, conventional strategies intended to decouple these quantities, including nanostructuring, solid-solution alloying, and defect engineering, have generally produced only limited improvements in ZT. The underlying issue is an inherent trade-off: phonon scattering introduced to reduce the lattice thermal conductivity also tends to weaken phonon drag, while the associated disorder reduces the exceptionally high carrier mobility that underpins the electrical conductivity of $FeSb_2$. Consequently, the power factor is often reduced more rapidly than the thermal conductivity. This interplay poses a central challenge for $FeSb_2$: how to suppress heat transport without significantly compromising the phonon-drag contribution and carrier mobility that together produce the large power factor. The aforementioned disputed experimental phenomena — particularly the characteristic resistivity transition, the magnetic susceptibility peak resembling that of SmB_6/FeSi, and the concomitantly occurring giant thermoelectric effect and high thermal conductivity at low temperatures — collectively form a complex puzzle. Any theory attempting to explain the microscopic mechanism of $FeSb_2$ must uniformly address a core question: what is the fundamental physical mechanism driving the profound reconstruction of its electronic state? Current discussions primarily revolve around two competing paradigms: i) The Kondo lattice picture views $FeSb_2$ as a correlated semiconductor or KI. ii) The spin-state excitation picture propose that the spin-state of the Fe ions may changes with temperature. These two theoretical paradigms offer distinct yet self-consistent physical pictures for understanding the exotic properties of $FeSb_2$. In the following sections, we will first delve into how the Kondo model explains these phenomena, drawing comparisons with typical KI like SmB_6 (Section 3). Subsequently, we will examine the theoretical predictions and experimental evidence for the spin-state excitation model, particularly direct insights provided by recent spectroscopic studies (Section 4), aiming to provide a clear perspective insight of the prolonged debate surrounding the microscopic origin of $FeSb_2$.

3 The physics of phase transition: An analogy to Kondo insulators

Metal–insulator-like transitions in compounds with partially filled d shells can arise from multiple microscopic mechanisms, including Slater- or Peierls-type instabilities and Mott physics. In $FeSb_2$, however, the emergence of a small low-temperature gap together with a crossover in the magnetic response points to a correlation-driven renormalization of the low-energy electronic structure. These observations have motivated the proposal that $FeSb_2$ may be analogous to Kondo insulators, a framework originally developed for f-electron heavy-fermion systems, where hybridization and many-body coherence produce a narrow gap. In this section, we review and critically assess the evidence for a KI-like interpretation of $FeSb_2$, and compare its key experimental signatures with those of established KI materials to clarify both the advantage and the limitations of this analogy.

3.1 The Kondo insulator analogy: Experimental evidence

The KI model describes materials in which a lattice of localized magnetic moments (typically from rare-earth f or transition-metal d orbitals) interacts with itinerant conduction electrons [62–68]. At high temperatures, the localized moments behave incoherently, leading to paramagnetic metallic state [Fig. 4(a)]. Upon cooling below a characteristic coherence temperature, the localized moments become screened by the conduction electrons, forming a non-magnetic spin-singlet ground state [Fig. 4(b)] [69]. This process opens a narrow hybridization gap at the Fermi level, driving a transition to an insulating state [Fig. 4(c)]. Owing to its striking experimental signatures, $FeSb_2$ has been widely discussed as a candidate for the extension of this theoretical framework to d-electron-based systems [52, 70].

Within the KI description, the resistivity evolution

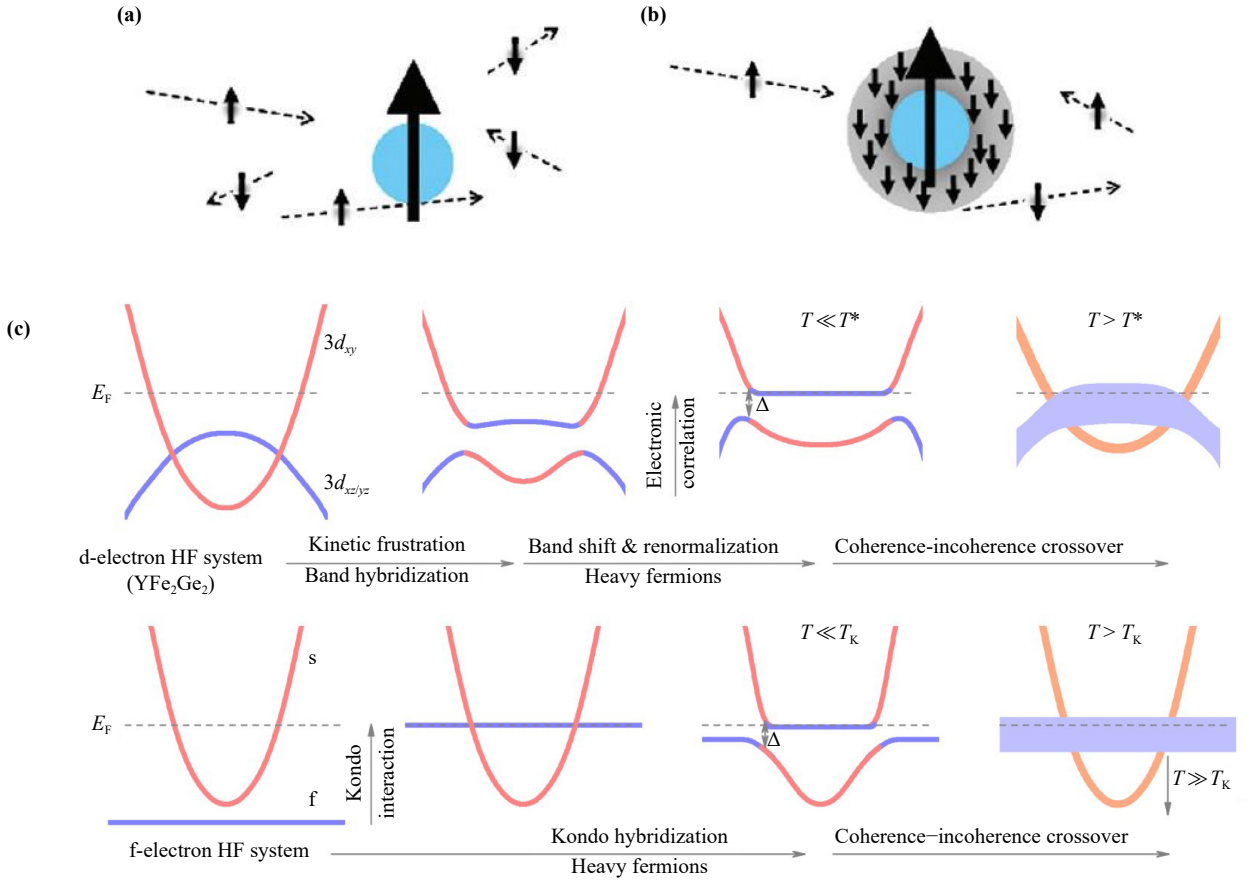

Fig. 4 **(a)** Schematic illustration of the high temperature regime ($T > T_K$) of the Kondo effect, where a magnetic impurity behaves approximately as a localized magnetic moment weakly coupled to a sea of conduction electrons. **(b)** Schematic illustration of the low temperature regime ($T < T_K$), where an antiferromagnetic exchange coupling between the impurity and conduction electrons leads to the formation of a Kondo screening cloud and the effective screening of the impurity moment. Reproduced from Ref. [69]. **(c)** Schematic comparison of how a flat band and a hybridization gap develop near the Fermi level in *d*-electron and *f*-electron systems, respectively. Reproduced from Ref. [67].

with temperature of $FeSb_2$ can be understood as a sequence of different transport regimes governed by the formation of the hybridization gap. The larger gap Δ_1, observed at higher temperatures ($T > 30$ K), is generally associated with the intrinsic band gap of the electronic structure. The smaller gap Δ_2, which dominates the transport at lower temperatures ($T < 30$ K), is often identified with the many-body hybridization gap itself. This energy scale reflects the strength of the Kondo hybridization and is regarded as a hallmark of KI-like behavior in $FeSb_2$ [70]. Furthermore, while the Kondo model alone cannot account for the large Seebeck coefficient observed in $FeSb_2$, the hybridization gives rise to sharp resonant features in the density of states near the narrow energy gap. This electronic structure, when strongly coupled to lattice vibrations through a phonon-drag mechanism, is widely considered responsible for the unusually large thermopower [56]. However, to further assess the applicability of the KI model, it is instructive to compare $FeSb_2$ with established KI.

3.2 Comparison with other Kondo insulators

While the Kondo model provides a coherent basis for interpreting the magnetic and electric phase transition in $FeSb_2$, direct comparison with well-established KIs such as SmB_6 reveals both striking parallels and critical distinctions that complicate a straightforward classification.

SmB_6, the prototypical *f*-electron KI with non-trivial topology, manifests Kondo correlation-driven insulating behavior [71–77]. It is featured with the coexistence of a correlated insulating bulk states and robust topological metallic surface states that dominate transport at low temperatures, a phenomenon confirmed by Angle-resolved photoemission spectroscopy (ARPES) and various transport measurements [Figs. 5(a, b)] [72, 73, 78, 79]. Intriguingly, ARPES measurements on $FeSb_2$ have revealed an electronic band structure surprisingly similar to that of SmB_6, identifying in-gap surface states that cross the Fermi level and a quasi-flat band located beneath the Fermi level through the facet of $FeSb_2$ (010)

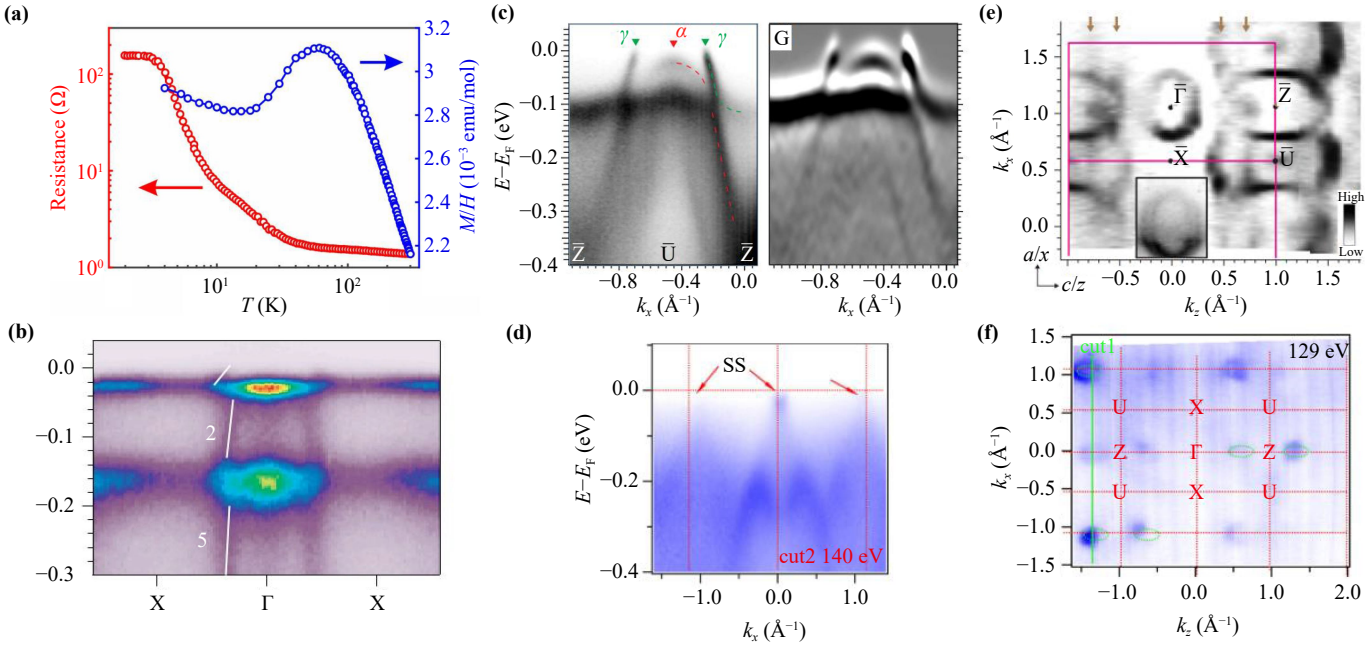

Fig. 5 **(a)** Temperature dependence of the resistivity and magnetic susceptibility of SmB6. The resistivity exhibits exponential increase upon cooling from room temperature, closely resembling the characteristic transport behavior observed in $FeSb_2$. Reproduced from Refs. [73, 77]. **(b)** The valence band spectra of SmB_6 along the X–Γ–X direction ($h\nu = 70$ eV) [72]. **(c)** The ARPES experiment of $FeSb_2$ observed surface states crossing the Fermi level on $\bar{Z}$–$\bar{U}$–$\bar{Z}$ direction, indicative of a metallic state [38]. **(d)** Another ARPES spectra along X–Γ–X taken at cuts 1 in (f), where SS denotes surface states. Reproduced from Ref. [48]. **(e)** Isoenergy mapping at Fermi energy (E_f) of $FeSb_2$ on the (010) surface, measured at 15 K with 70 eV photons. The surface Brillouin zone and high-symmetry points are indicated. The strong spectral weight near E_f highlights rich metallic surface states on this surface. Reproduced from Ref. [38]. **(f)** Another isoenergy mapping at E_f of $FeSb_2$ on the (010) surface, only weak and sporadic band crossings near E_f are observed, likely reflecting surface-termination/reconstruction effects rather than robust intrinsic surface states. Reproduced from Ref. [48].

[Figs. 5(c, d)]. While the overall phenomenology resembles that of SmB_6, the quasi-flat band in $FeSb_2$ originates from the weakly dispersive *d*-orbital states rather than *f*-electron states [38, 48]. Complementary transport experiments, including the previously discussed Corbino-disk geometry experiments, further support a scenario of an insulating bulk coexisting with a metallic surface channel [47]. However, both the origin of the gap and the nature of the in-gap states on the $FeSb_2$ (010) surface remain unsettled, owing to significant inconsistencies among ARPES studies. For example, Xu *et al.* [38] reported pronounced surface-derived features on the (010) surface and interpreted them as evidence for a KI-like hybridization gap with topologically nontrivial surface states [Fig. 5(e)]. In contrast, Chikina *et al.* [48] observed in-gap states with totally different dispersion and Fermiology, which were successfully interpreted as the trivial unbonded surface bands by calculations [Fig. 5(f)]. Taken together, the currently available surface-sensitive ARPES data suggest the surface states are highly sample-dependent, thus do not provide conclusive support for a topological Kondo-insulator picture in $FeSb_2$. This uncertainty motivates the use of bulk-sensitive probes, such as XAS, to establish the intrinsic electronic and magnetic evolution of the system and to distinguish between competing microscopic scenarios.

Furthermore, the gap observed in $FeSb_2$ (30–40 meV) is substantially larger than the hybridization gap typically reported for prototypical *f*-electron Kondo insulators such as SmB_6 (10–15 meV). Whereas the Kondo gap in SmB_6 is closely tied to the coherence temperature and becomes strongly thermally perturbed at temperatures of only a few tens of Kelvin, the gap in $FeSb_2$ remains robust over a much broader temperature range, extending to nearly room temperature. More importantly, if $FeSb_2$ were a conventional KI, its charge and spin responses would be expected to arise from the same underlying hybridization mechanism. However, the experimental results indicate a clear separation between these two channels: the magnetic susceptibility of $FeSb_2$ exhibits a pronounced crossover near 100 K, whereas the electrical resistivity shows no corresponding anomaly at that temperature. This mismatch between the transport and magnetic energy scales is difficult to reconcile with a conventional KI picture.

A more rigorous distinction between *d*- and *f*-electron systems also requires consideration of the hierarchy between spin-orbit coupling (SOC) and the crystal electric

field (CEF). In *f*-electron systems, SOC is intrinsically strong because of the large atomic number of rare-earth elements and typically defines the dominant local energy scale. For example, in Ce-based heavy-fermion compounds with a $4f^1$ configuration, the SOC splitting is typically on the order of 0.25–0.3 eV, whereas the CEF splitting is usually below 100 meV [80]. Consequently, the non-magnetic ground state in these materials emerges from the collective many-body Kondo screening process, while CEF effects mainly modify the fine level structure. By contrast, in *d*-electron systems such as $FeSb_2$, the more spatially extended 3d orbitals couple strongly to the ligand environment, making the crystal field the dominant energy scale. For Fe $3d$ states in $FeSb_2$, the effective crystal-field splitting is on the order of 1–2 eV, far exceeding the intrinsic SOC (~ 50 meV). Such a large crystal-field splitting favors a paired, diamagnetic low-spin ground state at the single-ion level, from which thermally activated spin-state excitations can occur.

In light of these fundamental differences, the classification of $FeSb_2$ as a genuine Kondo insulator remains under active debate. For example, several studies have shown that an insulating ground state can be reproduced from local Coulomb interactions among Fe $3d$ orbitals, without invoking Kondo hybridization [81, 82]. These ongoing debates have prompted the exploration of alternative mechanisms, such as temperature-driven spin-state excitations, which will be discussed in the next section.

4 The spin-state excitation paradigm

As discussed in the previous section, although the KI model could provide a phenomenologically consistant analogy for certain macroscopic observations, whether genuine many-body Kondo coherence exists in $FeSb_2$ remains controversial. These open questions have prompted the exploration of alternative microscopic mechanisms. Among them, the spin-state excitation (SSE) model has emerged as a promising framework, providing a more direct microscopic explanation for the anomalous physical properties of this *d*-electron system without invoking heavy-fermion hybridization.

SSE has been observed in transition metal compounds, particularly in systems based on $3d$ elements with near degenerate spin configurations [Fig. 6(a)] [83–86]. In these materials, partially filled *d*-orbitals on transition-metal ions (e.g., Fe or Co) may manifest more than one spin state — typically low-spin (LS) and high-spin (HS) configurations — which are nearly degenerate in energy. The ground states are mainly governed by the energy scale of the crystal electric field, which plays more prominent role in an insulator [Fig. 6(a)] [87]. Transitions between these states can be induced by external stimuli such as temperature, pressure, or magnetic fields, and light, which overcome the multiplet energy gap between the LS/HS. These distinct spin states exhibit different properties: LS state is nonmagnetic ($S = 0$) and has smaller effective ionic radius, while HS state possesses finite magnetic moments ($S > 0$) and a larger ionic volume [Fig. 6(b)] [88–90]. A temperature-driven spin-state crossover thus provides a possible mechanism by which a nonmagnetic, insulating ground state evolves into a paramagnetic and typically more conductive state at higher temperatures.

A prototypical SSE system is $LaCoO_3$, which crystallizes in a distorted perovskite structure with Co^{3+} ions in an octahedral (CoO_6) environment and a $3d^6$ electronic configuration, analogous to Fe^{2+} ($3d^6$) in octahedral $FeSb_6$ units in $FeSb_2$ [Fig. 6(c)]. It has been studied for decades to understand its SSE induced magnetic transition. $LaCoO_3$ displays a magnetic and metal-insulator crossover that can be understood in terms of thermally driven transitions from a LS ground state to HS state [Fig. 6(d)] [90–94]. Spectroscopic studies, including XAS and inelastic scatterings (RIXS) by Haverkort *et al.* [95], have provided smoking-gun evidence for such transitions. Further work by Takegami *et al.* [89] highlighted the critical role of lattice relaxation in enabling the thermal population of spin-excited states and successfully reproducing the observed temperature dependence.

A similar crystal field scenario may be applicable to $FeSb_2$, where Fe ions reside in a distorted octahedral environment, similar to the Co ions in $LaCoO_3$. In such a field, the $3d$ orbitals split into lower energy t_{2g} and higher-energy e_g levels [87]. When the crystal field splitting energy is comparable to the Hund's exchange energy of the $3d$-orbitals, the energy difference between the LS and HS would be shrinked, enabling thermally activated transitions between LS and HS configurations. Unlike the KI model, which requires coherent hybridization over extended length scales, the SSE model emphasizes local thermal excitations. This allows for a correlated but localized interpretation of the temperature evolution of both resistivity and magnetic susceptibility, without invoking long-range electronic coherence. Moreover, the pronounced transport anisotropy observed in $FeSb_2$ — which is difficult to reconcile with the KI model — can emerge in the SSE framework: the crystal-field splitting that determines the LS-HS energy separation is inherently sensitive to structural distortions and bonding geometry [44, 96]. Consequently, anisotropic thermal lattice distortions naturally lead to axis-dependent transport properties. Thus, the SSE model provides a self-consistent narrative that captures multiple key features of $FeSb_2$ and merits consideration alongside Kondo descriptions.

Nevertheless, the SSE framework remains under experimental scrutiny. For instance, inelastic neutron scattering (INS) studies by Zaliznyak *et al.* [97] did not observe spin-related excitations within 60 meV corresponding to LS-HS transitions at low temperature, but leaving signals between 15 meV to 30 meV not easy to

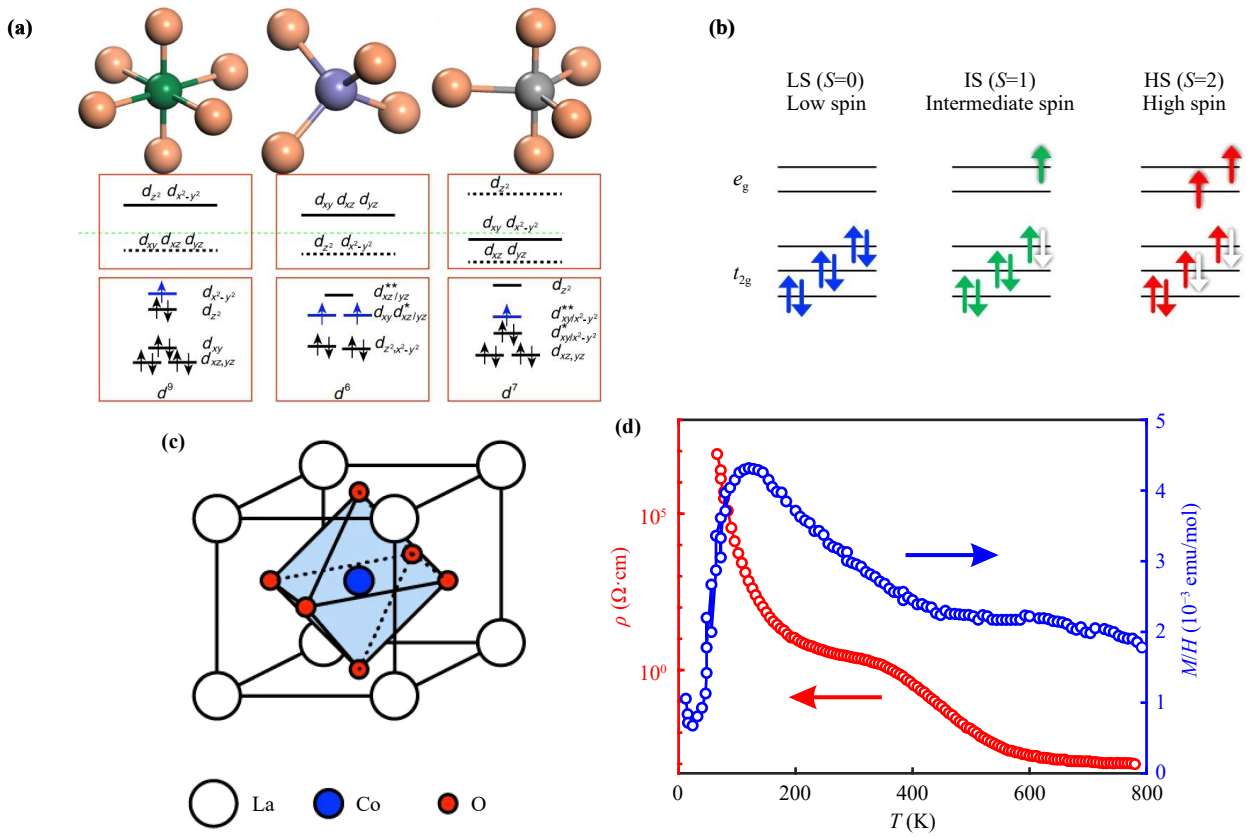

Fig. 6 **(a)** Structural units and the corresponding crystal field splitting of cation d orbitals in three representative coordination geometries: octahedral, tetrahedral, and trigonal bipyramidal. Reproduced from Ref. [87]. **(b)** Schematic spin-state configurations of Co^{3+} ($3d^6$) in $LaCoO_3$. In a strong octahedral crystal field, the low-spin (LS) state corresponds to six electrons paired in the t_{2g} manifold ($t_{2g}^6 e_g^0$), while intermediate spin (IS) and high spin (HS) states involve thermally excited electrons promoted to the eg levels, leading to partially unpaired configurations with increasing total spin [90]. **(c)** Crystal structure of $LaCoO_3$. The schematic highlights the CoO_6 octahedra. This local coordination environment is analogous to the $FeSb_6$ units in $FeSb_2$, supporting the application of similar crystal-field models [90]. **(d)** Temperature dependence of the electrical resistivity (red line) and magnetic susceptibility (blue line) of a $LaCoO_3$ single crystal, illustrating a magnetic and metal-insulator-like crossover. This behavior is commonly discussed in terms of thermally driven spin-state excitation from a low-spin (LS) ground state toward higher-spin states at elevated temperatures, providing a useful reference for comparison with $FeSb_2$. Reproduced from Ref. [94].

interpret. High-field Mössbauer spectroscopy on $FeSb_2$ by Farhan *et al.* [98] have reported the presence of two distinct Fe sites with different hyperfine parameters, which hinted two different spin components from a single valence condition. Moreover, direct spectroscopic evidence confirming temperature dependent spin state transitions in $FeSb_2$ remains lacking, leaving the actual role of the SSE model in $FeSb_2$ unconfirmed. The next section will examine available spectroscopic studies of $FeSb_2$ in greater detail, assessing whether experimental data can help distinguish between competing theoretical pictures.

5 X-ray absorption evidence for spin-state excitations in $FeSb_2$

The transport and magnetic measurements of $FeSb_2$ can be qualitatively captured by two fundamentally different models: the Kondo hybridization framework and the SSE picture. As outlined in Section 4, previous spectroscopic studies failed to resolve this issue, and in some cases even deepened the debate. In this context, XAS, a technique highly sensitive to both the valence state and local spin configuration of transition metal ions [99], provides a promising route to probe this problem. A recent study conducted a systematic Fe $3d$ L-edge XAS study on $FeSb_2$, combined with atomic multiplet simulations (AMS), to investigate the spin state configuration of Fe in high quality $FeSb_2$ single crystals [100].

By comparing experimental spectra to AMS simulations, it was found that the Fe valence was confirmed to be in a $3d^6$ configuration [Fig. 7(a)]. A pure low-spin (LS, S = 0) state successfully captured the overall spectral shape, but failed to account for key pre-edge peak structures observed near the L_3 and L_2 edges. These features could

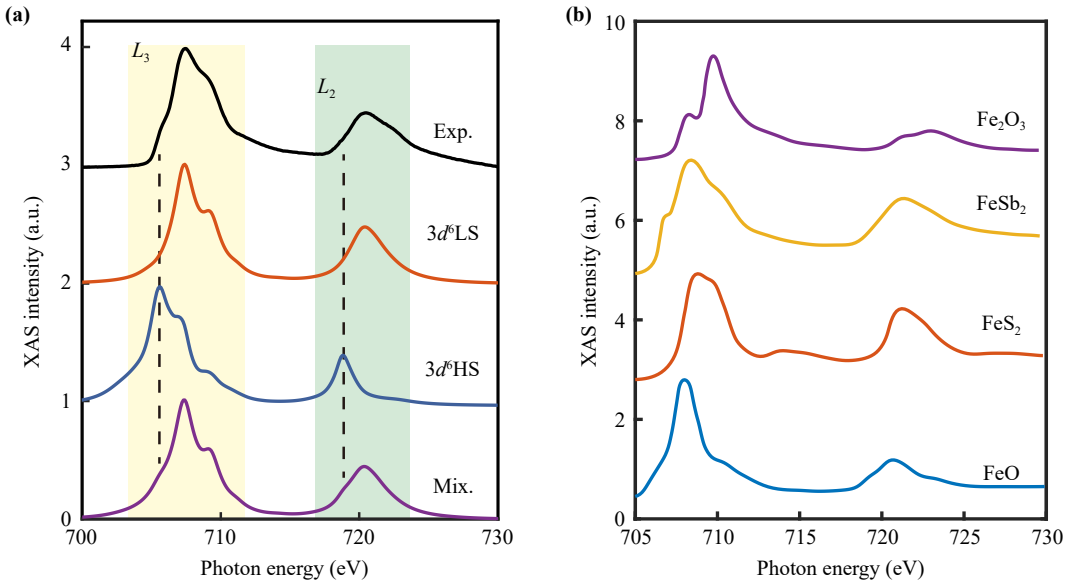

Fig. 7 **(a)** The comparison of Fe L-edge XAS curves between experiments (black, $T = 20$ K) and the simulations of $3d^6$ LS state (red), HS state (blue), and the mixed spin state (purple, with 15% HS). Reproduced from Ref. [100]. **(b)** The L-edge XAS results in different compounds. Reproduced from Ref. [51]. The distinct variation in spectral features highlights the sensitivity of the XAS technique to the local chemical environment and the specific valence state of the Fe ions.

not be attributed to alternative valence states (e.g., $3d^4$ or $3d^5$), but emerged naturally when a high-spin (HS, S = 2) state component was introduced into the simulation. Similar to the XAS results reported by Sun *et al.* [51] for various iron-based compounds, the data suggest the possible existence of distinct spin states in $FeSb_2$ [Fig. 7(b)]. A mixed spin state simulation (composed of 85% LS and 15% HS) yielded excellent agreement with the full experimental spectrum, including the pre-edge peaks. This may provide the direct spectroscopic evidence that the ground state of $FeSb_2$ is not a pure nonmagnetic LS state, but a correlated mixture of LS and HS configurations.

Further evidence comes from temperature dependent XAS experiments. In the process of ramping up the temperature of $FeSb_2$ sample from 20 K to 300 K, the overall spectral profile did not change significantly, but difference spectra (subtracting the 20 K data) reveal systematic evolution [Figs. 8(a, b)]. Specifically, the spectral feature (peak) at the energies associated with HS states (e.g., ~ 705.7 eV) gradually gains the intensity, while the loss of spectral intensity (dip) are observed at LS related features (~ 707.5 eV and ~ 709.4 eV). This peak-dip pattern in the differential spectra provides evidence for a thermal redistribution of spin populations from LS state to HS state. AMS simulations confirm that increasing the HS fraction from approximately 15% to ~20% reproduces these spectral changes quantitatively [Fig. 8(c)]. This result links the macroscopic transition of $FeSb_2$ with a microscopic increase in thermally activated HS occupancy [Fig. 8(d)].

A potential concern is that the properties of topological correlated materials may differ between surface and bulk. Given the surface-sensitive nature of XAS in the total electron yield (TEY) mode, it is necessary to determine whether the SSE features originate from the surface states previously detected by ARPES on (010) facets [38, 48] or from the intrinsic bulk properties. To address this ambiguity, the study employed ARPES measurement to characterize the (001) facet of $FeSb_2$. In contrast to the $FeSb_2$ (010) facet, which hosts metallic surface states, the (001) facet shows no quasiparticle intensity at $E = E_F$ (Fermi level) [Fig. 9(a)]. ARPES cuts along high symmetry directions reveal a band gap of ~ 30–40 meV, consistent with the activation gap Δ_1 observed in bulk transport measurements [Figs. 9(b–e)]. This established the (001) facet as an ideal, surface-states-free platform for a control experiment, on which temperature-dependent XAS measurements were repeated. The resulting XAS response and its temperature evolution were found to be nearly identical to those measured on the (010) facet. These results strongly indicating that the SSE is intrinsic to the bulk, rather than a surface dominated feature.

The presence of surface states on the (010) facet has previously been taken as evidence supporting a topological Kondo narrative of $FeSb_2$, while the absence of surface state on the (001) facet implicates the trivial topology of $FeSb_2$. As a bulk-surface correspondence, the non-trivial topology would give rise to surface state on any facet that breaks translational symmetry, which is not relying on specific facet. Thus, the identification of surface-state-free (001) facet also unambiguously exclude the assumption

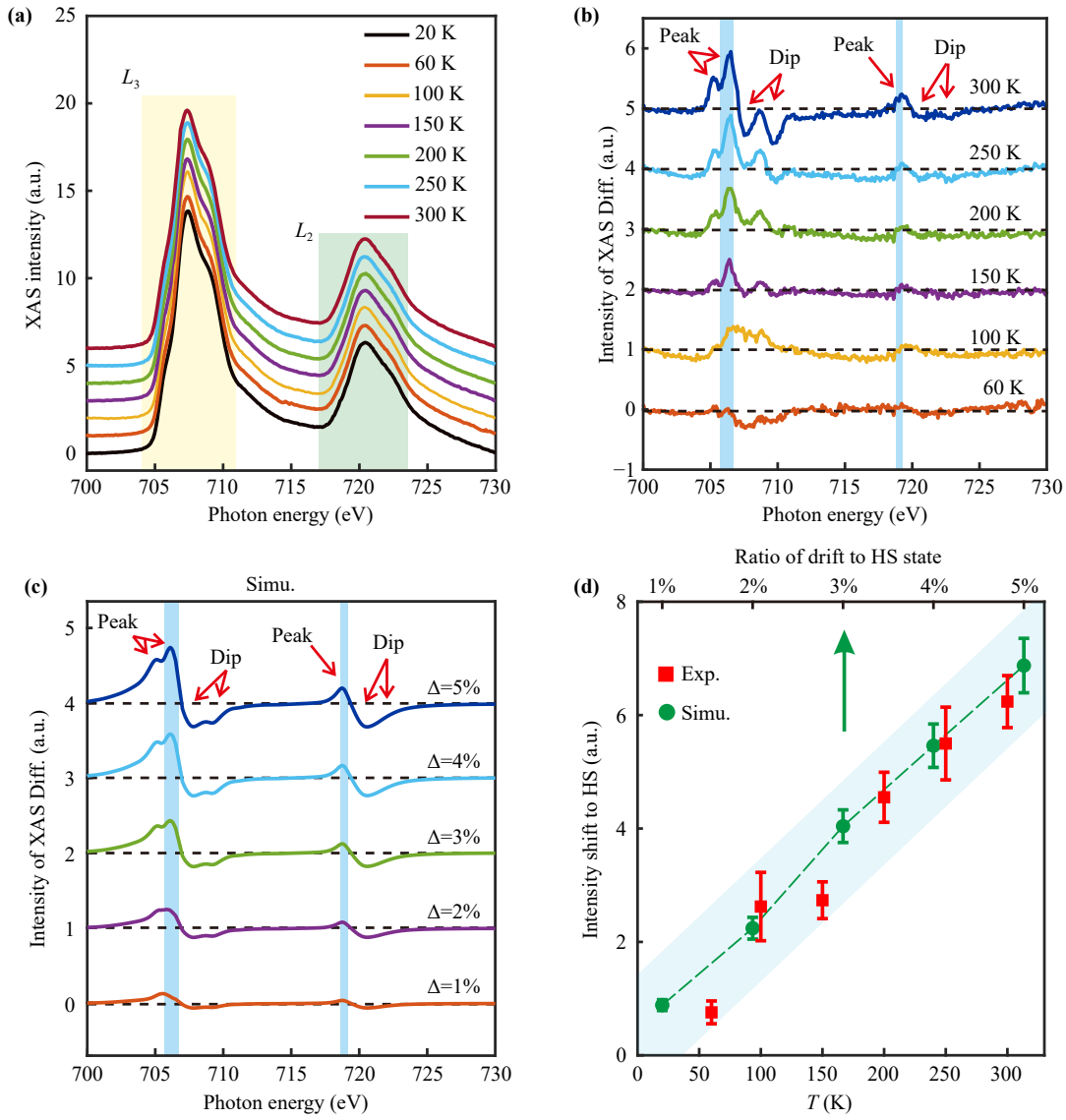

Fig. 8 **(a)** The XAS curves of $FeSb_2$ at different temperatures, showing only very minor changes in the overall line shape upon heating. **(b)** The temperature-dependent differentiated XAS curves after subtracting the XAS curve of $T = 20$ K (I_T–$I_{20\,K}$), revealing clear temperature-dependent intensity redistribution with distinct positive and negative features, indicative of thermally activated changes in the electronic configuration. **(c)** The simulated differentiated XAS curves after subtracting the XAS curve with 15% HS state, which successfully capture the main temperature-dependent modifications observed in the experiment. **(d)** The XAS intensities shifted from the LS state to the HS state extracted from experiments (red) and simulations (green) (left axis), and the corresponding ratio of HS state populated from low temperature to 300 K (top axis). Reproduced from Ref. [100].

of non-trivial topology in $FeSb_2$.

To further explore the tunability of spin states, the effects of doping were studied. $RuSb_2$ is isostructural with $FeSb_2$ and thus offers a way to chemically tune the electronic environment without introducing significant structural disorder. At 20 K, the 5% Ru-doped $FeSb_2$ exhibited stronger pre-edge HS features in the XAS spectrum [Fig. 10(a)]. AMS fitting confirmed an increased HS fraction (~25%), suggesting that Ru doping reduces the LS–HS energy gap [Fig. 10(b)]. These spectroscopic trends to be parallel with macroscopic transport data, which show that Ru doping decreases the activation gap and enhances low-temperature conductivity.

First principles calculation gives an insight to the physical origin of the spin-state transition and the doping effect [Figs. 10(c, d)]. For instance, Density functional theory (DFT)-based calculations confirmed again that LS state and HS state of $3d^6$ in $FeSb_2$ are energetically almost degenerate. The energy difference of the ground state between the two states is about 7 meV, which is rather comparable to the thermal excitation of ~ 100 K. Moreover, this energy scale is sensitive to the SOC

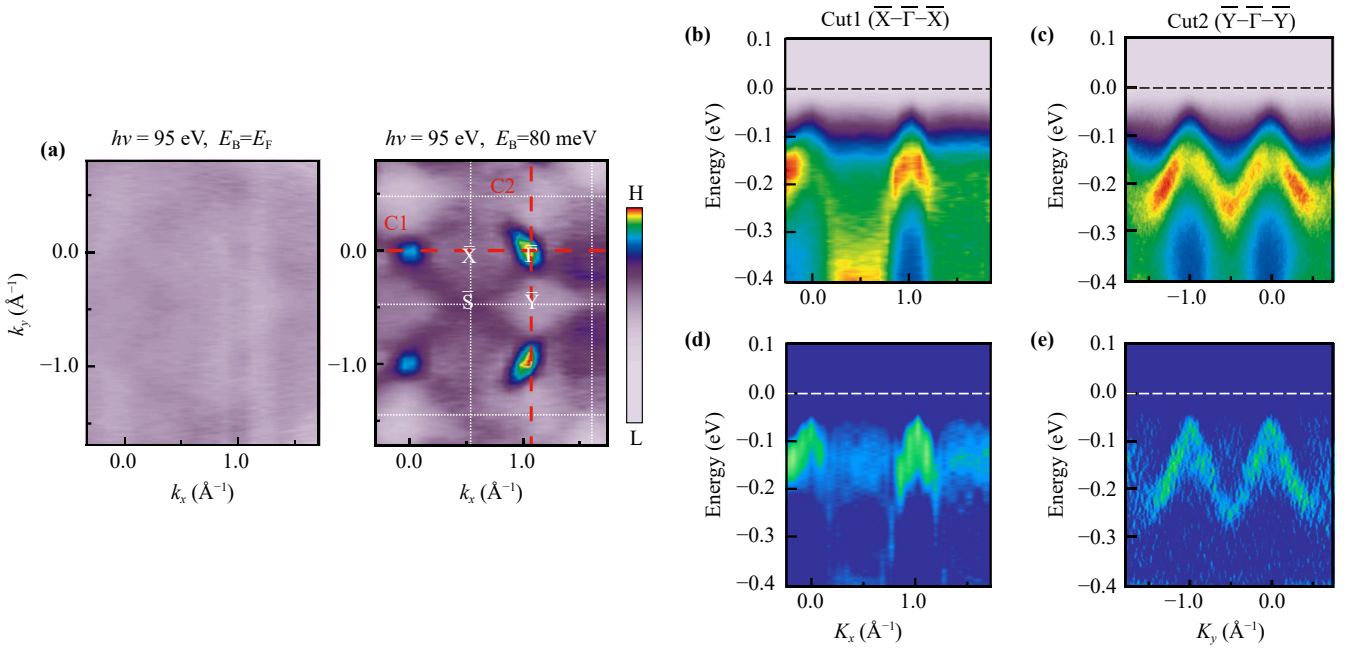

Fig. 9 The ARPES measurements of $FeSb_2$ (001). **(a)** The energy contour cuts at Fermi level and E_B = 80 meV (hv = 95 eV). White dashed lines note the 2D Brillouin zone. **(b, c)** ARPES taken along $\bar{X}$–$\bar{\Gamma}$–$\bar{X}$ direction and $\bar{Y}$–$\bar{\Gamma}$–$\bar{Y}$ direction, with corresponding second derivative images in **(d)** and **(e)** to highlight the band dispersions. Reproduced from Ref. [100].

energy. The substitution with a heavy element would eliminate the ground state energy difference. According to the calculations, replacing Fe with Ru can further lowers the HS energy level and promotes HS occupancy, regardless how the Hubbard U or Hund's coupling J values are tuned, clearly illustrate why HS-state is populated through Ru-doping.

Although first-principles calculations capture the near-degeneracy of spin states and the trend induced by Ru substitution, $FeSb_2$ has shown intriguing and, at times, contradictory behavior in DFT-based calculations. These discrepancies in the resulting ground states are often taken as indications of strong-correlation or spin-fluctuation effects beyond static mean-field theory, but they can also arise from the extreme sensitivity of narrow-gap systems in first-principles calculations. Specifically, the metallic and magnetic ground state reported in certain studies (e.g., Refs. [30, 101]) was obtained using the standard PBE-GGA (generalized gradient approximation (GGA) of the Perdew–Burke–Ernzerhof (PBE)) functional. It is well known that PBE systematically underestimates the band gaps of semiconductors [102–104]. Because the experimental band gap of $FeSb_2$ is exceptionally small (30–40 meV), well below the typical uncertainty of standard DFT functionals (~ 0.1–0.2 eV), PBE could artificially close the gap and thus yield a spurious metallic state. By contrast, gap-correcting approaches such as the modified Becke–Johnson (mBJ) potential can recover a small gap; however, the resulting electronic structure remains highly sensitive to small changes in the computational parameters. Because the target gap lies near the limit of computational precision, different methods, or even minor variations in computational parameters, can easily tip the balance and lead to qualitatively different outcomes (metallic versus semiconducting, or magnetic versus non-magnetic). Consequently, although these contrasting theoretical results underscore the complexity of $FeSb_2$, they should be interpreted with caution, and intrinsic physical mechanisms should be carefully distinguished from the methodological limitations inherent in describing extremely narrow gaps.

In summary, the XAS and ARPES measurement provide essential spectroscopic evidence for spin-state excitation in $FeSb_2$, supporting a ground state comprising a mixture of low spin and high spin Fe^{2+} configurations. The temperature dependent and Ru-doping dependent evolution of the high spin fraction correlates closely with macroscopic transport trends, reinforcing the relevance of spin-state physics in this system. The experimental and theoretical analysis further suggests that crystal field splitting and Hund's coupling alone are insufficient to determine the spin state hierarchy. SOC, which energetically favors the high spin state, plays a non-negligible role. For a given SOC strength, the delicate balance between CEF and Hund's coupling can be thermally tuned when the LS and HS states are nearly degenerate, leading to the observed redistribution of spin populations and transition behaviors.

However, while the AMS simulations captures key spectral features and provides a useful model for interpreting XAS data, it remains a simplified toy-model that

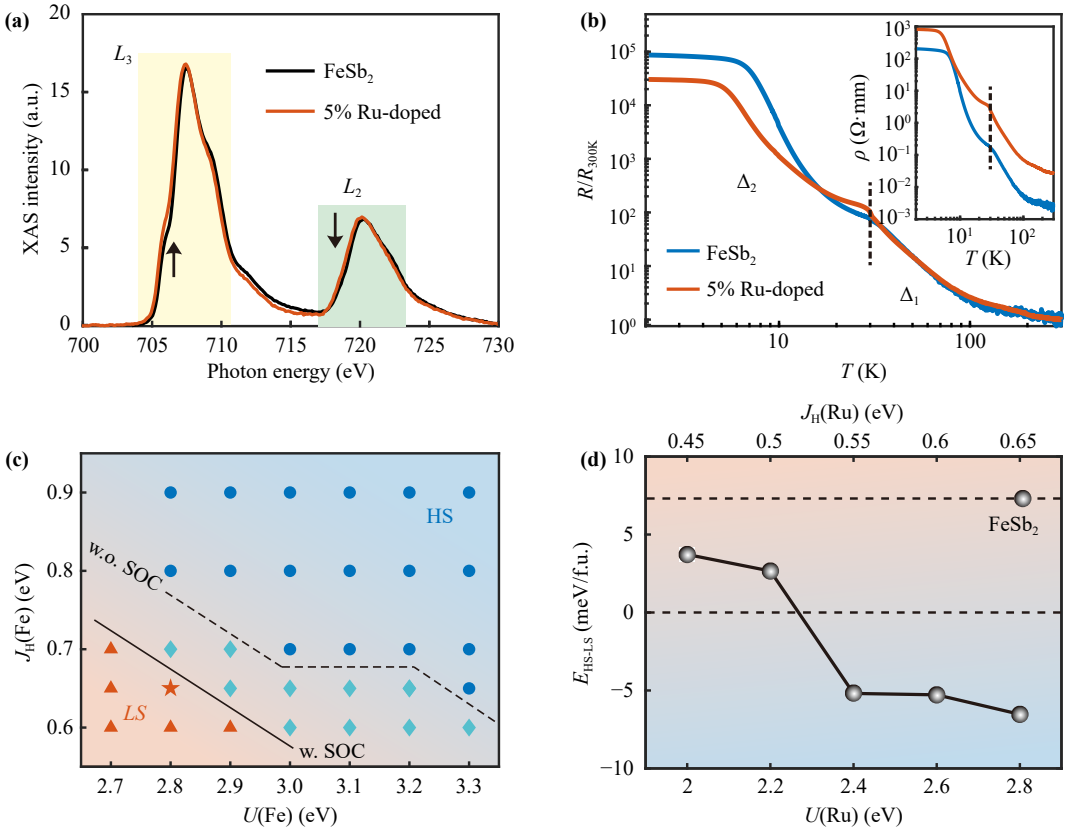

Fig. 10 **(a)** The XAS curves of $FeSb_2$ and Ru-doped $FeSb_2$ at $T = 20$ K. **(b)** The normalized resistance (R/R_{300K}) of $FeSb_2$ and $Fe_{0.95}Ru_{0.05}Sb_2$ as a function of temperature. **(c)** The spin-state phase diagram of $FeSb_2$ in the parameter space of Fe's U and J_H. The blue dots (red triangles) indicate that the ground state is the HS (LS) state regardless of whether the spin–orbit coupling (SOC) effect is taken into account. The cyan diamonds indicate a transition region where the ground state is the LS state without SOC but the HS state with SOC. The red star indicates the selected U and J_H when calculating Ru-doping. **(d)** The energy difference between the HS and LS states changes with the Ru-dopants' U/J_H values. Reproduced from Ref. [100].

does not provide an exact quantitative description of the complex solid environment. Moreover, the small energy scale associated with these spin state transitions presents a significant challenge for theoretical treatment, requiring high precision models capable of resolving fine balance between correlation, spin–orbit interaction, and lattice dynamics. Future work combining high-resolution spectroscopy with advanced theoretical approaches will be highly desired for fully resolving the microscopic origin of $FeSb_2$'s spin state behavior and its role in the material's anomalous properties.

6 Summary and outlook

Through decades of investigation, $FeSb_2$ has been known a compelling model system at the intersection of electronic correlated physics and functional materials science. This review has examined the material's unusual transition properties and two competing theoretical interpretations: the KI explanation and the SSE narrative. The accumulated evidence, especially the most recent ARPES and XAS work, clearly substantiate the magnetic transition, as well as the transport anomaly is directly derived from the SSE mechanism. The exclusion of the KI candidate makes the resistivity saturation and 2D transport nature of the cryogenic regime still an open question. However, it is important to emphasize that there is no theorem which excludes the coexistence of the spin-state excitation and Kondo hybridization. While current bulk sensitive evidence firmly establishes SSE as the dominant driver of the anomalous temperature evolution, we cannot fully rule out a coexistence or coupled scenario. It is highly plausible that a Kondo-like coherence or hybridization at low temperatures subtly contributes to stabilizing the low-spin ground state through correlation-driven renormalization. As temperature increases, the suppression of this coherence may in turn facilitate the thermal population of higher spin states. Future investigations may still need to consider whether elements of Kondo interactions play a subtle role in these unresolved low-temperature phenomena.

However, as we discussed before, the energy scales of the interactions of CEF and SOC within *d*-orbital and *f*-orbital are totally different. Whether or not the single-ion impurity model could extend to a Kondo lattice coherence in the materials of *d*-orbital basis is very interesting.

We notice that upon doping, $FeSb_2$ has recently been discussed as a candidate of altermagnet, which would manifest the spin-splitting band structure under the time-reversal symmetry preservation [101, 105–107]. We are convinced that understanding the spin configuration, as well as the low-energy electronic band structure is vital in advancing the both new altermagnetic physics and thermoelectricity-oriented applications. To finish this review, we provide a brief perspective on both aspects.

Thermoelectric optimization. One of the core challenges in $FeSb_2$ research is resolving the so-called "thermoelectric dilemma": the coexistence of an exceptionally large power factor and a high lattice thermal conductivity, which limits the thermoelectric figure of merit. Various strategies have been attempted to address this issue. Elemental doping (e.g., Bi, Te) has been shown to suppress thermal conductivity but also reduces electrical conductivity and power factor, resulting in limited ZT enhancement [108, 109]. Substitutions of both Fe (e.g., Co, Cr) sites have been explored, with limited improvement in enhancing thermoelectric performance [110]. These reports highlight a general dilemma in doping strategies: reducing lattice thermal conductivity often comes at the expense of carrier mobility and electronic performance. An alternative approach has focused on fabricating the thin films devices. For instance, magnetron sputtered $FeSb_2$ films with controlled Sb vacancies show reduced thermal conductivity but inferior power factor compared to single crystals [111]; MBE-grown films allow exploration of phonon drag effects and heterostructure engineering, enhancing the thermopower to 208 μV/K [112]. Other efforts focus on defect engineering in single crystals to enhance phonon scattering while minimizing disruption to electronic transport [59–61, 113–116]. Although ZT value of 0.071 has been achieved in $FeSb_2$ at 55 K [111], the challenge for practical application remains significant. These efforts collectively involve different efforts to tune the thermoelectricity, including chemically doping, alloying, or nanostructuring (e.g., thin films, nanowires, composites) [109, 117–123] aiming at selectively scattering phonons without degrading carrier mobility. In parallel, theoretical studies and high throughput screening may aid in identifying optimal doping or design strategies. A deeper understanding of the phonon drag mechanism and its coupling to spin and electronic structure will be essential [58, 124–127].

Altermagnetism. Altermagnetism is a recently proposed class of materials characterized by momentum-dependent spin-splitting despite vanishing net magnetization, attracting attention for their potential applications in spintronics [128–135]. Although $FeSb_2$ itself is nonmagnetic, its distinctive crystal symmetry is potential to break the PT-symmetry to host the exotic magnetic order. Recent theoretical works repeatly proposed that doping $FeSb_2$ (e.g., with Co) could induce AFM order and derive an altermagnetic phase in this system [101]. Experimentally verifying this prediction presents a compelling research direction, requiring a combination of magnetization measurements and advanced spectroscopic techniques (such as spin-resolved ARPES or XMCD) to map the magnetic phase diagram and spin textures of doped $FeSb_2$. Confirming altermagnetism in this system would not only expand the family of known altermagnetic materials, but also position $FeSb_2$ as a potential platform for next-generation spintronic devices.

In conclusion, $FeSb_2$ continues to stand out as a unique platform linking narrow-gap semiconductors, strongly correlated electron systems, and high-performance thermoelectric materials. Deepening the understanding of the interplay between electronic correlations, spin states, lattice dynamics, and potential exotic magnetic order in this material may not only resolve its underlying physical puzzles, but also push forward the frontier of research for next-generation materials with enhanced energy-conversion efficiency and spintronic functionalities.

Declarations The authors declare that they have no competing interests and there are no conflicts.

Acknowledgements This work was supported by the National Key R&D Program of China (No. 2022YFA1405700), the National Natural Science Foundation of China (No. 12374058), the Basic Research Program of Jiangsu (Grant No BK20250071). X.Z. was supported by the National Natural Science Foundation of China (Grant No. 12404127), the Natural Science Foundation of Jiangsu Province (Grant No. BK20241262), the Fundamental Research Funds for the Central Universities (Grant No. 2242025K30023), the Start-up Research Fund of Southeast University (No. RF1028624083), and the Open Research Fund of Key Laboratory of Quantum Materials and Devices (Southeast University), Ministry of Education.

References

1. J. M. Tomczak, Thermoelectricity in correlated narrow-gap semiconductors, *J. Phys.: Condens. Matter* 30(18), 183001 (2018)
2. P. Cheng and Y. Yang, Narrowing the band gap: The key to high-performance organic photovoltaics, *Acc. Chem. Res.* 53(6), 1218 (2020)
3. F. Xia, H. Wang, D. Xiao, M. Dubey, and A. Ramasubramaniam, Two-dimensional material nanophotonics, *Nat. Photonics* 8(12), 899 (2014)
4. A. Rogalski, Scaling infrared detectors — status and outlook, *Rep. Prog. Phys.* 85(12), 126501 (2022)

5. J. Yao and G. Yang, 2D material broadband photodetectors, *Nanoscale* 12(2), 454 (2020)
6. D. Yang and D. Ma, Development of organic semiconductor photodetectors: From mechanism to applications, *Adv. Opt. Mater.* 7(1), 1800522 (2019)
7. J. Zheng, H. Zhou, Y. Zou, R. Wang, Y. Lyu, S. P. Jiang, and S. Wang, Efficiency and stability of narrow-gap semiconductor-based photoelectrodes, *Energy Environ. Sci.* 12(8), 2345 (2019)
8. S. Gielen, C. Kaiser, F. Verstraeten, J. Kublitski, J. Benduhn, D. Spoltore, P. Verstappen, W. Maes, P. Meredith, A. Armin, and K. Vandewal, Intrinsic detectivity limits of organic near-infrared photodetectors, *Adv. Mater.* 32(47), 2003818 (2020)
9. X. Yu, Y. Li, X. Hu, D. Zhang, Y. Tao, Z. Liu, Y. He, M. A. Haque, Z. Liu, T. Wu, and Q. J. Wang, Narrow bandgap oxide nanoparticles coupled with graphene for high performance mid-infrared photodetection, *Nat. Commun.* 9(1), 4299 (2018)
10. X. H. Li, Y. X. Guo, Y. Ren, J. J. Peng, J. S. Liu, C. Wang, and H. Zhang, Narrow-bandgap materials for optoelectronics applications, *Front. Phys. (Beijing)* 17(1), 13304 (2021)
11. J. Yue, J. Zhang, L. Qin, F. Meng, Y. Jiang, R. Wen, L. Zhao, Z. Zhang, Y. Jiang, C. Du, H. Jia, H. Chen, W. Wang, and Z. Deng, Mid-wave infrared polarization detection through an InSb detector integrated with subwavelength aluminum gratings, *Infrared Phys. Technol.* 152, 106183 (2026)
12. E. Delli, V. Letka, P. D. Hodgson, E. Repiso, J. P. Hayton, A. P. Craig, Q. Lu, R. Beanland, A. Krier, A. R. J. Marshall, and P. J. Carrington, Mid-infrared InAs/InAsSb superlattice nBn photodetector monolithically integrated onto silicon, *ACS Photonics* 6(2), 538 (2019)
13. D. Hsieh, Y. Xia, D. Qian, L. Wray, F. Meier, J. H. Dil, J. Osterwalder, L. Patthey, A. V. Fedorov, H. Lin, A. Bansil, D. Grauer, Y. S. Hor, R. J. Cava, and M. Z. Hasan, Observation of time-reversal-protected single-Dirac-cone topological-insulator states in Bi_2Te_3 and Sb_2Te_3, *Phys. Rev. Lett.* 103(14), 146401 (2009)
14. T. Fang, X. Li, C. Hu, Q. Zhang, J. Yang, W. Zhang, X. Zhao, D. J. Singh, and T. Zhu, Complex band structures and lattice dynamics of Bi_2Te_3-based compounds and solid solutions, *Adv. Funct. Mater.* 29(28), 1900677 (2019)
15. P. Ghaemi, R. S. K. Mong, and J. E. Moore, In-plane transport and enhanced thermoelectric performance in thin films of the topological insulators Bi_2Te_3 and Bi_2Se_3, *Phys. Rev. Lett.* 105(16), 166603 (2010)
16. D. W. Ao, W. D. Liu, Y. X. Chen, M. Wei, B. Jabar, F. Li, X. L. Shi, Z. H. Zheng, G. X. Liang, X. H. Zhang, P. Fan, and Z. G. Chen, Novel thermal diffusion temperature engineering leading to high thermoelectric performance in Bi_2Te_3-based flexible thin-films, *Adv. Sci. (Weinh.)* 9(5), 2103547 (2022)
17. M. Scheele, N. Oeschler, K. Meier, A. Kornowski, C. Klinke, and H. Weller, Synthesis and thermoelectric characterization of Bi_2Te_3 nanoparticles, *Adv. Funct. Mater.* 19(21), 3476 (2009)
18. N. Xu, Y. Xu, and J. Zhu, Topological insulators for thermoelectrics, *NPJ Quantum Mater.* 2(1), 51 (2017)
19. A. Bentien, S. Johnsen, G. K. H. Madsen, B. B. Iversen, and F. Steglich, Colossal Seebeck coefficient in strongly correlated semiconductor $FeSb_2$, *Europhys. Lett.* 80(1), 17008 (2007)
20. A. Bentien, G. K. H. Madsen, S. Johnsen, and B. B. Iversen, Experimental and theoretical investigations of strongly correlated $FeSb_{2-x}Sn_x$, *Phys. Rev. B* 74(20), 205105 (2006)
21. R. Hu, V. F. Mitrović, and C. Petrovic, Giant carrier mobility in single crystals of $FeSb_2$, *Appl. Phys. Lett.* 92(18), 182108 (2008)
22. Y. Sun, S. Johnsen, P. Eklund, M. Sillassen, J. Bøttiger, N. Oeschler, P. Sun, F. Steglich, and B. B. Iversen, Thermoelectric transport properties of highly oriented $FeSb_2$ thin films, *J. Appl. Phys.* 106(3), 033710 (2009)
23. Y. Sun, E. Zhang, S. Johnsen, M. Sillassen, P. Sun, F. Steglich, J. Bøttiger, and B. B. Iversen, Growth of $FeSb_2$ thin films by magnetron sputtering, *Thin Solid Films* 519(16), 5397 (2011)
24. H. Takahashi, R. Okazaki, Y. Yasui, and I. Terasaki, Low-temperature magnetotransport of the narrow-gap semiconductor $FeSb_2$, *Phys. Rev. B* 84(20), 205215 (2011)
25. A. Datta and G. S. Nolas, Synthesis and characterization of nanocrystalline $FeSb_2$ for thermoelectric applications, *Eur. J. Inorg. Chem.* 2012(1), 55 (2012)
26. J. Janaki, A. Mani, A. T. Satya, T. G. Kumary, S. Kalavathi, and A. Bharathi, Influence of Ni doping on the electrical and structural properties of $FeSb_2$, *Phys. Status Solidi B* 249(9), 1756 (2012)
27. A. Mani, J. Janaki, T. G. Kumary, D. K. Baisnab, and A. Bharathi, Thickness-dependent electrical resistivity evolution in $Fe_{1-x}Ni_xSb_2$ thin films, *Solid State Commun.* 194, 30 (2014)
28. K. Wei, J. Martin, and G. S. Nolas, Synthesis, SPS processing and low temperature transport properties of polycrystalline $FeSb_2$ with nano-scale grains, *Mater. Lett.* 122, 289 (2014)
29. Q. Du and C. Petrovic, Optimal carrier concentration for $FeSb_2$ colossal thermopower, *Appl. Phys. Lett.* 118(23), 233901 (2021)
30. S. Malki, L. El Farh, A. Challioui, and M. Zanouni, A first-principles investigation on electronic structure and optical properties of tetragonal iron antimonide $FeSb_2$, *J. Supercond. Nov. Magn.* 35(6), 1507 (2022)
31. D. Gujjar, S. Gujjar, V. K. Malik, and H. C. Kandpal, Transport and electrical properties of cryogenic thermoelectric $FeSb_2$: The effect of isoelectronic and hole doping, *J. Phys.: Condens. Matter* 36(11), 115703 (2024)
32. A. G. Eaton, et al., Electrical transport signatures of metallic surface state formation in the strongly-correlated insulator $FeSb_2$, arXiv: 2403.04550 (2024)
33. J. A. Horn, Y. S. Eo, K. Avers, H. Yoon, R. G. Dorman, S. R. Saha, and J. Paglione, Magnetocrystalline anisotropy and 3D hopping conduction at the surface of $FeSb_2$, arXiv: 2509.05788 (2025)
34. M. Zhang, S. Dai, R. Zhang, M. Shu, W. Xu, J. Zhu, X. Liu, Y. Luo, and B. T. Ishigaki, Lattice and phonon

properties in semiconductors $FeSb_2$ and $RuSb_2$, *Chin. Phys. B* 34(8), 086302 (2025)
35. X. Feng, L. K. Ang, S. A. Yang, C. Xiao, and X. C. Xie, Giant out-of-plane magnetic orbital torque of altermagnets from spin-group symmetry breaking, arXiv: 2602.19076 (2026)
36. J. A. Horn, K. E. Avers, N. Crombie, S. R. Saha, and J. Paglione, Anisotropic magnetism at the surface of a non-magnetic bulk insulator, arXiv: 2602.16557 (2026)
37. A. G. Eaton, $FeSb_2$: A riddle, inside an insulator, wrapped in a metal electric and magnetic properties of the unconventional insulator iron diantimonide, *Apollo-University of Cambridge Repository*, doi: 10.17863/CAM.91726 (2022)
38. K. J. Xu, S. Chen, Y. He, J. He, S. Tang, C. Jia, E. Yue Ma, S. Mo, D. Lu, M. Hashimoto, T. P. Devereaux, and Z. Shen, Metallic surface states in a correlated d-electron topological kondo insulator candidate $FeSb_2$, *Proc. Natl. Acad. Sci. USA* 117(27), 15409 (2020)
39. S. Hong, P. Ghaemi, J. E. Moore, and P. W. Phillips, Tuning thermoelectric power factor by crystal-field and spin-orbit couplings in kondo-lattice materials, *Phys. Rev. B* 88(7), 075118 (2013)
40. Q. Jie, R. Hu, E. Bozin, A. Llobet, I. Zaliznyak, C. Petrovic, and Q. Li, Electronic thermoelectric power factor and metal–insulator transition in $FeSb_2$, *Phys. Rev. B* 86(11), 115121 (2012)
41. P. Sun, N. Oeschler, S. Johnsen, B. B. Iversen, and F. Steglich, Narrow band gap and enhanced thermoelectricity in $FeSb_2$, *Dalton Trans.* 39(4), 1012 (2010)
42. C. Petrovic, J. W. Kim, S. L. Bud'ko, A. I. Goldman, P. C. Canfield, W. Choe, and G. J. Miller, Anisotropy and large magnetoresistance in the narrow-gap semiconductor $FeSb_2$, *Phys. Rev. B* 67(15), 155205 (2003)
43. M. A. Kassem, Y. Tabata, T. Waki, and H. Nakamura, Crystal growth and metallic ferromagnetism induced by electron doping in $FeSb_2$, arXiv: 2011.10343 (2020)
44. C. C. Homes, Q. Du, C. Petrovic, W. H. Brito, S. Choi, and G. Kotliar, Unusual electronic and vibrational properties in the colossal thermopower material $FeSb_2$, *Sci. Rep.* 8(1), 11692 (2018)
45. P. Sun, M. Søndergaard, B. Iversen, and F. Steglich, Strong electron correlations in $FeSb_2$, *Ann. Phys.* 523(8-9), 612 (2011)
46. P. Sun, N. Oeschler, S. Johnsen, B. B. Iversen, and F. Steglich, $FeSb_2$: Prototype of huge electron-diffusion thermoelectricity, *Phys. Rev. B* 79(15), 153308 (2009)
47. Y. S. Eo, K. Avers, J. A. Horn, H. Yoon, S. R. Saha, A. Suarez, M. S. Fuhrer, and J. Paglione, Extraordinary bulk-insulating behavior in the strongly correlated materials FeSi and $FeSb_2$, *Appl. Phys. Lett.* 122(23), 233102 (2023)
48. A. Chikina, J. Z. Ma, W. H. Brito, S. Choi, P. Sémon, A. Kutepov, Q. Du, J. Jandke, H. Liu, N. C. Plumb, M. Shi, C. Petrovic, M. Radovic, and G. Kotliar, Correlated electronic structure of colossal thermopower $FeSb_2$: An ARPES and ab initio study, *Phys. Rev. Res.* 2(2), 023190 (2020)
49. R. Hu, R. P. Hermann, F. Grandjean, Y. Lee, J. B. Warren, V. F. Mitrović, and C. Petrovic, Weak ferromagnetism in $Fe_{1-x}Co_xSb_2$, *Phys. Rev. B* 76(22), 224422 (2007)
50. T. Deguchi, K. Matsubayashi, Y. Uwatoko, T. Koyama, T. Kohara, H. Nakamura, Y. Mitsui, and K. Koyama, Magnetic measurements of narrow-gap semiconductor $FeSb_2$ under high pressure, *Mater. Trans.* 61(8), 1476 (2020)
51. P. Sun, et al., Magnetism and spin states of $FeSb_2$, Max Planck Institute for Chemical Physics of Solids, Sci. Rep. 55 (2011)
52. Z. Schlesinger, Z. Fisk, H. T. Zhang, and M. B. Maple, Is FeSi a Kondo insulator? *Physica B* 237–238, 460 (1997)
53. S. Paschen, E. Felder, M. A. Chernikov, L. Degiorgi, H. Schwer, H. R. Ott, D. P. Young, J. L. Sarrao, and Z. Fisk, Low-temperature transport, thermodynamic, and optical properties of FeSi, *Phys. Rev. B* 56(20), 12916 (1997)
54. P. Sun, W. Xu, J. M. Tomczak, G. Kotliar, M. Søndergaard, B. B. Iversen, and F. Steglich, Highly dispersive electron relaxation and colossal thermoelectricity in the correlated semiconductor $FeSb_2$, *Phys. Rev. B* 88(24), 245203 (2013)
55. P. Sun, N. Oeschler, S. Johnsen, B. B. Iversen, and F. Steglich, Thermoelectric properties of the narrow-gap semiconductors $FeSb_2$ and $RuSb_2$, *J. Phys. Conf. Ser.* 150(1), 012049 (2009)
56. H. Takahashi, R. Okazaki, S. Ishiwata, H. Taniguchi, A. Okutani, M. Hagiwara, and I. Terasaki, Colossal Seebeck effect enhanced by quasi-ballistic phonons dragging massive electrons in $FeSb_2$, *Nat. Commun.* 7(1), 12732 (2016)
57. J. M. Tomczak, K. Haule, T. Miyake, A. Georges, and G. Kotliar, Thermopower of correlated semiconductors: Application to $FeAs_2$ and $FeSb_2$, *Phys. Rev. B* 82(8), 085104 (2010)
58. M. Battiato, J. M. Tomczak, Z. Zhong, and K. Held, Unified picture for the colossal thermopower compound $FeSb_2$, *Phys. Rev. Lett.* 114(23), 236603 (2015)
59. R. Masuki, T. Nomoto, and R. Arita, Origin of anomalous temperature dependence of the Nernst effect in narrow-gap semiconductors, *Phys. Rev. B* 103(4), L041202 (2021)
60. H. Matsuura, H. Maebashi, M. Ogata, and H. Fukuyama, Effect of phonon drag on Seebeck coefficient based on linear response theory: Application to $FeSb_2$, *J. Phys. Soc. Jpn.* 88(7), 074601 (2019)
61. M. Pokharel, H. Zhao, K. Lukas, Z. Ren, C. Opeil, and B. Mihaila, Phonon drag effect in nanocomposite $FeSb_2$, *MRS Commun.* 3(1), 31 (2013)
62. S. Rachel, Interacting topological insulators: A review, *Rep. Prog. Phys.* 81(11), 116501 (2018)
63. M. Neupane, N. Alidoust, S. Y. Xu, T. Kondo, Y. Ishida, D. J. Kim, C. Liu, I. Belopolski, Y. J. Jo, T. R. Chang, H. T. Jeng, T. Durakiewicz, L. Balicas, H. Lin, A. Bansil, S. Shin, Z. Fisk, and M. Z. Hasan, Surface electronic structure of the topological Kondo-insulator candidate correlated electron system SmB_6, *Nat. Commun.* 4(1), 2991 (2013)
64. M. Dzero, K. Sun, V. Galitski, and P. Coleman, Topo-

logical Kondo insulators, *Phys. Rev. Lett.* 104(10), 106408 (2010)
65. Z. Fisk, J. L. Sarrao, J. D. Thompson, D. Mandrus, M. F. Hundley, A. Miglori, B. Bucher, Z. Schlesinger, G. Aeppli, E. Bucher, J. F. DiTusa, C. S. Oglesby, H. R. Ott, P. C. Canfield, and S. E. Brown, Kondo insulators, *Physica B* 206–207, 798 (1995)
66. A. M. Strydom, A review of the kondo insulator materials class of strongly correlated electron systems: Selected systems and anomalous behavior, *Front. Phys. (Lausanne)* 11, 11 (2023)
67. B. Xu, R. Liu, H. Wo, Z. Liao, S. Yi, C. Li, J. Zhao, X. Qiu, Z. Yin, and C. Bernhard, Unraveling the origin of kondo-like behavior in the 3D-electron heavy-fermion compound YFe_2Ge_2, *Proc. Natl. Acad. Sci. USA* 121(39), e2401430121 (2024)
68. Y. Kim, M. Kim, M. S. Kim, C. W. Cheng, J. Choi, S. Jung, D. Lu, J. H. Kim, S. Cho, D. Song, D. Oh, L. Yu, Y. J. Choi, H. D. Kim, J. H. Han, Y. Jo, J. H. Shim, J. Seo, S. Huh, and C. Kim, Kondo interaction in FeTe and its potential role in the magnetic order, *Nat. Commun.* 14(1), 4145 (2023)
69. G. D. Scott and D. Natelson, Kondo resonances in molecular devices, *ACS Nano* 4(7), 3560 (2010)
70. C. Petrovic, Y. Lee, T. Vogt, N. Dj. Lazarov, S. L. Bud'ko, and P. C. Canfield, Kondo insulator description of spin state transition in $FeSb_2$, *Phys. Rev. B* 72(4), 045103 (2005)
71. L. Li, K. Sun, C. Kurdak, and J. W. Allen, Emergent mystery in the Kondo insulator samarium hexaboride, *Nat. Rev. Phys.* 2(9), 463 (2020)
72. J. D. Denlinger, J. W. Allen, J. S. Kang, K. Sun, B. Min, D. J. Kim, and Z. Fisk, SmB_6 photoemission: Past and present, arXiv: 1312.6636 (2013)
73. D. J. Kim, J. Xia, and Z. Fisk, Topological surface state in the kondo insulator samarium hexaboride, *Nat. Mater.* 13(5), 466 (2014)
74. M. Dzero, J. Xia, V. Galitski, and P. Coleman, Topological Kondo insulators, *Annu. Rev. Condens. Matter Phys.* 7(7), 249 (2016)
75. H. Weng, J. Zhao, Z. Wang, Z. Fang, and X. Dai, Topological crystalline kondo insulator in mixed valence ytterbium borides, *Phys. Rev. Lett.* 112(1), 016403 (2014)
76. A. S. Panfilov, V. A. Desnenko, A. A. Lyogenkaya, G. E. Grechnev, and N. Yu. Shitsevalova, Probing the bulk valence of Sm in SmB_6 by studying the magnetic susceptibility under pressure, *Low Temp. Phys.* 49(9), 1037 (2023)
77. K. Akintola, A. Pal, S. R. Dunsiger, A. C. Y. Fang, M. Potma, S. R. Saha, X. Wang, J. Paglione, and J. E. Sonier, Freezing out of a low-energy bulk spin exciton in SmB_6, *npj Quantum Mater.* 3(1), 36 (2018)
78. N. Xu, X. Shi, P. K. Biswas, C. E. Matt, R. S. Dhaka, Y. Huang, N. C. Plumb, M. Radović, J. H. Dil, E. Pomjakushina, K. Conder, A. Amato, Z. Salman, D. M. K. Paul, J. Mesot, H. Ding, and M. Shi, Surface and bulk electronic structure of the strongly correlated system SmB_6 and implications for a topological Kondo insulator, *Phys. Rev. B* 88(12), 121102 (2013)
79. Y. Ohtsubo, Y. Yamashita, K. Hagiwara, S. Ideta, K. Tanaka, R. Yukawa, K. Horiba, H. Kumigashira, K. Miyamoto, T. Okuda, W. Hirano, F. Iga, and S. Kimura, Non-trivial surface states of samarium hexaboride at the (111) surface, *Nat. Commun.* 10(1), 2298 (2019)
80. G. Zhao, H. Li, W. Lin, Q. Ren, J. Denlinger, Y. D. Chuang, X. Zhang, L. A. Wray, and L. Miao, Determination of the crystal-field splitting of the $4f^4$ state in samarium-alloyed cerium hexaboride, *Phys. Rev. B* 107(24), 245149 (2023)
81. J. Kuneš and V. I. Anisimov, Temperature-dependent correlations in covalent insulators: Dynamical mean-field approximation, *Phys. Rev. B.* 78(3), 033109 (2008)
82. A. Bentien, G. K. H. Madsen, S. Johnsen, and B. B. Iversen, Experimental and theoretical investigations of strongly correlated $Fe_2Sb_{2-x}Sn_x$, *Phys. Rev. B* 74(20), 205105 (2006)
83. K. Tomiyasu, J. Okamoto, H. Y. Huang, Z. Y. Chen, E. P. Sinaga, W. B. Wu, Y. Y. Chu, A. Singh, R. P. Wang, F. M. F. de Groot, A. Chainani, S. Ishihara, C. T. Chen, and D. J. Huang, Coulomb correlations intertwined with spin and orbital excitations in $LaCoO_3$, *Phys. Rev. Lett.* 119(19), 196402 (2017)
84. M. A. Halcrow, Trapping and manipulating excited spin states of transition metal compounds, *Chem. Soc. Rev.* 37(2), 278 (2008)
85. M. Imada, A. Fujimori, and Y. Tokura, Metal-insulator transitions, *Rev. Mod. Phys.* 70(4), 1039 (1998)
86. S. Hayami, Z. Gu, M. Shiro, Y. Einaga, A. Fujishima, and O. Sato, First observation of light-induced excited spin state trapping for an iron(III) complex, *J. Am. Chem. Soc.* 122(29), 7126 (2000)
87. J. Hu, C. Le, and X. Wu, Predicting unconventional high-temperature superconductors in trigonal bipyramidal coordinations, *Phys. Rev. X* 5(4), 041012 (2015)
88. W. Zhang, R. Alonso-Mori, U. Bergmann, C. Bressler, M. Chollet, A. Galler, W. Gawelda, R. G. Hadt, R. W. Hartsock, T. Kroll, K. S. Kjær, K. Kubiček, H. T. Lemke, H. W. Liang, D. A. Meyer, M. M. Nielsen, C. Purser, J. S. Robinson, E. I. Solomon, Z. Sun, D. Sokaras, T. B. van Driel, G. Vankó, T. C. Weng, D. Zhu, and K. J. Gaffney, Tracking excited-state charge and spin dynamics in iron coordination complexes, *Nature* 509(7500), 345 (2014)
89. D. Takegami, A. Tanaka, S. Agrestini, Z. Hu, J. Weinen, M. Rotter, C. Schüßler Langeheine, T. Willers, T. C. Koethe, T. Lorenz, Y. F. Liao, K. D. Tsuei, H. J. Lin, C. T. Chen, and L. H. Tjeng, Paramagnetic $LaCoO_3$: A highly inhomogeneous mixed spin-state system, *Phys. Rev. X* 13(1), 011037 (2023)
90. A. Ikeda, Y. H. Matsuda, K. Sato, Y. Ishii, H. Sawabe, D. Nakamura, S. Takeyama, and J. Nasu, Signature of spin-triplet exciton condensations in $LaCoO_3$ at ultrahigh magnetic fields up to 600 T, *Nat. Commun.* 14(1), 1744 (2023)
91. T. Kyômen, Y. Asaka, and M. Itoh, Negative cooperative effect on the spin-state excitation in $LaCoO_3$, *Phys. Rev. B* 67(14), 144424 (2003)
92. A. Podlesnyak, S. Streule, J. Mesot, M. Medarde, E. Pomjakushina, K. Conder, A. Tanaka, M. W.

Haverkort, and D. I. Khomskii, Spin-state transition in $LaCoO_3$: Direct neutron spectroscopic evidence of excited magnetic states, *Phys. Rev. Lett.* 97(24), 247208 (2006)

93. E. J. Guo, R. Desautels, D. Lee, M. A. Roldan, Z. Liao, T. Charlton, H. Ambaye, J. Molaison, R. Boehler, D. Keavney, A. Herklotz, T. Z. Ward, H. N. Lee, and M. R. Fitzsimmons, Exploiting symmetry mismatch to control magnetism in a ferroelastic heterostructure, *Phys. Rev. Lett.* 122(18), 187202 (2019)
94. S. Yamaguchi, Y. Okimoto, H. Taniguchi, and Y. Tokura, Spin-state transition and high-spin polarons in $LaCo_3$, *Phys. Rev. B* 53(6), R2926 (1996)
95. M. W. Haverkort, Z. Hu, J. C. Cezar, T. Burnus, H. Hartmann, M. Reuther, C. Zobel, T. Lorenz, A. Tanaka, N. B. Brookes, H. H. Hsieh, H. J. Lin, C. T. Chen, and L. H. Tjeng, Spin state transition in $LaCoO_3$ studied using soft X-ray absorption spectroscopy and magnetic circular dichroism, *Phys. Rev. Lett.* 97(17), 176405 (2006)
96. C. J. Kang and G. Kotliar, Study for material analogs of $FeSb_2$: Material design for thermoelectric materials, *Phys. Rev. Mater.* 2(3), 034604 (2018)
97. I. A. Zaliznyak, A. T. Savici, V. O. Garlea, R. Hu, and C. Petrovic, Absence of localized-spin magnetism in the narrow-gap semiconductor $FeSb_2$, *Phys. Rev. B* 83(18), 184414 (2011)
98. A. Farhan, M. Reissner, A. Leithe-Jasper, and W. Steiner, A high-field Mössbauer investigation on $FeSb_2$, *J. Phys.: Conf. Ser.* 217(1), 012142 (2010)
99. M. Sakamaki and K. Amemiya, Nanometer-resolution depth-resolved measurement of florescence-yield soft X-ray absorption spectroscopy for FeCo thin film, *Rev. Sci. Instrum.* 88(8), 083901 (2017)
100. H. Li, G. Wang, N. Ding, Q. Ren, G. Zhao, W. Lin, J. Yang, W. Yan, Q. Li, R. Yang, S. Yuan, J. D. Denlinger, Z. Wang, X. Zhang, L. A. Wray, S. Dong, D. Qian, and L. Miao, Spectroscopic evidence of spin-state excitation in d-electron correlated semiconductor $FeSb_2$, *Proc. Natl. Acad. Sci. USA* 121(28), e2321193121 (2024)
101. I. I. Mazin, K. Koepernik, M. D. Johannes, R. González-Hernández, and L. Šmejkal, Prediction of unconventional magnetism in doped $FeSb_2$, *Proc. Natl. Acad. Sci. USA* 118(42), e2108924118 (2021)
102. X. Zheng, A. J. Cohen, P. Mori-Sánchez, X. Hu, and W. Yang, Improving band gap prediction in density functional theory from molecules to solids, *Phys. Rev. Lett.* 107(2), 026403 (2011)
103. J. M. Crowley, J. Tahir-Kheli, and W. A. I. III Goddard, Resolution of the band gap prediction problem for materials design, *J. Phys. Chem. Lett.* 7(7), 1198 (2016)
104. I. Jihad, M. H. S. Anfa, S. M. Alqahtani, and F. H. Alharbi, DFT-PBE band gap correction using machine learning with a reduced set of features, *Comput. Mater. Sci.* 244, 113153 (2024)
105. C. Phillips, G. Pokharel, K. Shtefiienko, S. R. Bhandari, D. E. Graf, D. P. Rai, and K. Shrestha, Electronic structure of the altermagnet candidate $FeSb_2$: High-field torque magnetometry and density functional theory studies, *Phys. Rev. B* 111(7), 075141 (2025)
106. A. Gauswami and P. K. Jha, Exploration of surface oriented altermagnetic states in CrTe, $FeSb_2$ and MnO_2: A first-principles study, *J. Phys.: Condens. Matter* 37(30), 305801 (2025)
107. M. Roig, A. Kreisel, Y. Yu, B. M. Andersen, and D. F. Agterberg, Minimal models for altermagnetism, *Phys. Rev. B* 110(14), 144412 (2024)
108. D. Gujjar, S. Gujjar, V. K. Malik, and H. C. Kandpal, Transport and electrical properties of cryogenic thermoelectric $FeSb_2$: The effect of isoelectronic and hole doping, *J. Phys.: Condens. Matter* 36(11), 115703 (2023)
109. P. Sun, M. Søndergaard, Y. Sun, S. Johnsen, B. B. Iversen, and F. Steglich, Unchanged thermopower enhancement at the semiconductor-metal transition in correlated $FeSb_{2-x}Te_x$, *Appl. Phys. Lett.* 98(7), 072105 (2011)
110. K. Wang, R. Hu, J. Warren, and C. Petrovic, Enhancement of the thermoelectric properties in doped $FeSb_2$ bulk crystals, *J. Appl. Phys.* 112(1), 013703 (2012)
111. J. Li, Z. Yang, D. S. Nkemeni, Y. Zhang, S. Lou, and S. Zhou, High thermoelectric figure of merit of $FeSb_{2-x}$ thin films via defect engineering for low-temperature cooling applications, *J. Electron. Mater.* 50(12), 6724 (2021)
112. C. Yamamoto, X. He, K. Hanzawa, T. Katase, M. Sasase, J. Yamaura, H. Hiramatsu, H. Hosono, and T. Kamiya, Phonon drag thermopower persisting over 200 K in $FeSb_2$ thin film on $SrTiO_3$ single crystal, *Appl. Phys. Lett.* 124(19), 193902 (2024)
113. Y. Wang, C. Fu, T. Zhu, L. Hu, G. Jiang, G. Zhao, D. Huo, and X. Zhao, Hot deformation induced defects and performance enhancement in $FeSb_2$ thermoelectric materials, *J. Appl. Phys.* 114(18), 184904 (2013)
114. Z. Chen, X. Ding, and M. Xu, Low thermal conductivity and magneto-suppressed thermal transport in a highly oriented $FeSb_2$ single crystal, *ACS Omega* 6(35), 22681 (2021)
115. Q. Du, L. Wu, H. Cao, C. J. Kang, C. Nelson, G. L. Pascut, T. Besara, T. Siegrist, K. Haule, G. Kotliar, I. Zaliznyak, Y. Zhu, and C. Petrovic, Vacancy defect control of colossal thermopower in $FeSb_2$, *npj Quantum Mater.* 6(1), 13 (2021)
116. H. Takahashi, Y. Yasui, I. Terasaki, and M. Sato, Effects of ppm-level imperfection on the transport properties of $FeSb_2$ single crystals, *J. Phys. Soc. Jpn.* 80(5), 054708 (2011)
117. M. Koirala, H. Zhao, M. Pokharel, S. Chen, T. Dahal, C. Opeil, G. Chen, and Z. Ren, Thermoelectric property enhancement by Cu nanoparticles in nanostructured $FeSb_2$, *Appl. Phys. Lett.* 102(21), 213111 (2013)
118. A. V. Sanchela, A. D. Thakur, and C. V. Tomy, Effects of S doping on the thermoelectric properties of $FeSb_2$, *Mater. Today Proc.* 67, 935 (2022)
119. G. Tan, W. Liu, H. Chi, X. Su, S. Wang, Y. Yan, X. Tang, W. Wong-Ng, and C. Uher, Realization of high thermoelectric performance in p-type unfilled ternary skutterudites $FeSb_{2+x}Te_{1-x}$ via band structure modifi-

cation and significant point defect scattering, *Acta Mater.* 61(20), 7693 (2013)

120. Q. Du, X. Tong, Y. Liu, and C. Petrovic, Suppression of thermal conductivity and electronic correlations in $Fe_{1-x}Ru_xSb_2$ ($0 \leq x \lesssim 0.6$), *Appl. Phys. Lett.* 118(17), 171904 (2021)
121. S. Zhu, W. Xie, D. Thompson, T. Holgate, M. Zhou, Y. Yan, and T. M. Tritt, Tuning the thermoelectric properties of polycrystalline $FeSb_2$ by the in situ formation of Sb/InSb nanoinclusions, *J. Mater. Res.* 26(15), 1894 (2011)
122. H. Zhao, M. Pokharel, G. Zhu, S. Chen, K. Lukas, Q. Jie, C. Opeil, G. Chen, and Z. Ren, Dramatic thermal conductivity reduction by nanostructures for large increase in thermoelectric figure-of-merit of $FeSb_2$, *Appl. Phys. Lett.* 99(16), 163101 (2011)
123. Y. Sun, S. Canulescu, P. Sun, F. Steglich, N. Pryds, J. Schou, and B. B. Iversen, Pulsed laser deposition growth of $FeSb_2$ films for thermoelectric applications, *Mater. Chem. Phys.* 129(1), 105 (2011)
124. M. S. Diakhate, R. P. Hermann, A. Möchel, I. Sergueev, M. Søndergaard, M. Christensen, and M. J. Verstraete, Thermodynamic, thermoelectric, and magnetic properties of $FeSb_2$: A combined first-principles and experimental study, *Phys. Rev. B* 84(12), 125210 (2011)
125. M. S. Figueira, J. Silva-Valencia, and R. Franco, Thermoelectric properties of the Kondo insulator $FeSb_2$, *Eur. Phys. J. B* 85(6), 203 (2012)
126. R. Miao, G. Huang, C. Fan, Z. Bai, Y. Li, L. Wang, L. Chen, W. Song, and Q. Xu, First-principles study on the lattice dynamics of $FeSb_2$, *Solid State Commun.* 152(3), 231 (2012)
127. B. Liao, S. Lee, K. Esfarjani, and G. Chen, First-principles study of thermal transport in $FeSb_2$, *Phys. Rev. B* 89(3), 035108 (2014)
128. L. Šmejkal, J. Sinova, and T. Jungwirth, Beyond conventional ferromagnetism and antiferromagnetism: A phase with nonrelativistic spin and crystal rotation symmetry, *Phys. Rev. X* 12(3), 031042 (2022)
129. L. Šmejkal, J. Sinova, and T. Jungwirth, Emerging research landscape of altermagnetism, *Phys. Rev. X* 12(3), 040501 (2022)
130. L. Bai, W. Feng, S. Liu, L. Šmejkal, Y. Mokrousov, and Y. Yao, Altermagnetism: Exploring new frontiers in magnetism and spintronics, *Adv. Funct. Mater.* 34(49), 2409327 (2024)
131. S. W. Cheong and F. T. Huang, Altermagnetism with non-collinear spins, *npj Quantum Mater.* 9(1), 13 (2024)
132. H. Bai, Y. C. Zhang, Y. J. Zhou, P. Chen, C. H. Wan, L. Han, W. X. Zhu, S. X. Liang, Y. C. Su, X. F. Han, F. Pan, and C. Song, Efficient spin-to-charge conversion via altermagnetic spin splitting effect in antiferromagnet RuO_2, *Phys. Rev. Lett.* 130(21), 216701 (2023)
133. X. Chen, J. Ren, Y. Zhu, Y. Yu, A. Zhang, P. Liu, J. Li, Y. Liu, C. Li, and Q. Liu, Enumeration and representation theory of spin space groups, *Phys. Rev. X* 14(3), 031038 (2024)
134. J. Ding, Z. Jiang, X. Chen, Z. Tao, Z. Liu, T. Li, J. Liu, J. Sun, J. Cheng, J. Liu, Y. Yang, R. Zhang, L. Deng, W. Jing, Y. Huang, Y. Shi, M. Ye, S. Qiao, Y. Wang, Y. Guo, D. Feng, and D. Shen, Large band splitting in g-wave altermagnet CrSb, *Phys. Rev. Lett.* 133(20), 206401 (2024)
135. Z. Zhou, X. Cheng, M. Hu, R. Chu, H. Bai, L. Han, J. Liu, F. Pan, and C. Song, Manipulation of the altermagnetic order in CrSb via crystal symmetry, *Nature* 638(8051), 645 (2025)